THE OCEAN IN THE CLIMATE SYSTEM: OBSERVING AND MODELING ITS VARIABILITY*

Thomas F. Stocker

Climate and Environmental Physics
Physics Institute, University of Bern
Sidlerstrasse 5, CH–3012 Bern, Switzerland
stocker@climate.unibe.ch, http://www.climate.unibe.ch

Abstract

The climate system consists of the five components atmosphere, ocean, cryophere, biosphere and lithosphere. In order to understand climate and its changes on timescales from decades to several 100,000 years, we need to focus on physical and geochemical processes particularly in the first four components. This chapter gives an introduction to the ocean component of the climate system. We first discuss the climatic relevance of the ocean not only as a thermal regulator but also as an important pacemaker of climate change. The dynamical principles of the large-scale ocean circulation are presented, and flow regimes relevant to climatic changes are explained. We then review results from models and observations that suggest that the cause for abrupt climatic changes, which are so abundant in the paleoclimatic record, is found in the ocean. The physical mechanisms for multiple equilibrium states of the thermohaline circulation are discussed. The ocean is also a pacemaker of decadal-to-century time scale variability. An overview of the evidence for natural variability based on various proxy data is given and a first attempt at a classification of mechanisms based on recent modeling results is made.

1 Climatic Relevance of the Ocean Circulation

The description and understanding of climate change and climate variability depends on our knowledge of the transport mechanisms and paths of energy, freshwater and substances through the different components of the climate system. Within a latitude band from about 40°S and 30°N the net radiative balance at the top of the atmosphere is positive whereas it is negative in the higher latitudes (Peixoto and Oort 1992). Thus, energy balance in the global climate system requires a meridional transport of energy from the equator to the pole in both hemispheres. The total amount of about 6 PW (1 PW=10^{15}W) is partitioned approximately equally among ocean and atmosphere (Figure 1).

While sensible and latent heat are carried in the atmosphere mainly by transient eddies (e.g., storms), transport of heat in the ocean is due to entirely different mechanisms as will become evident in this chapter. Unlike in the atmosphere, the ocean transports heat meridionally with a specific regional pattern. The depth-integrated meridional heat transport in the Pacific is nearly antisymmetric about the equator, i.e. heat is transported polewards in

*Current version: September 29, 2000. An earlier version appeared as Chapter 2 in: *Topics in Atmospheric and Interstellar Physics and Chemistry*, European Research Course on Atmospheres, Volume 2, edited by C. F. Boutron, Les Editions de Physique, Les Ulis, France, 1996, pages 39–90.

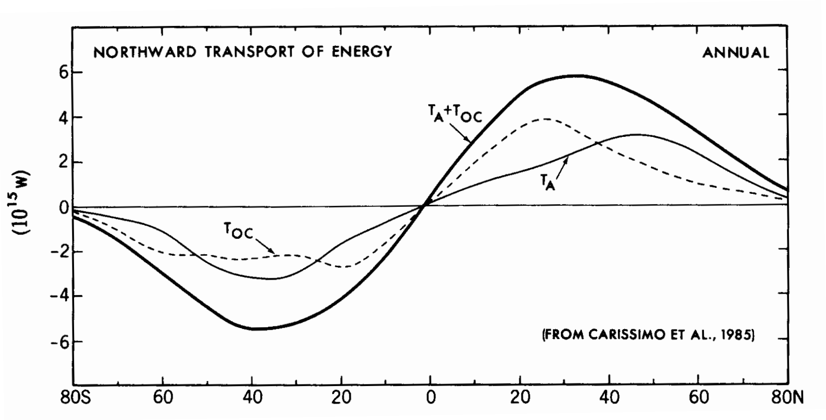

Figure 1: Annual mean meridional heat transport in the ocean and atmosphere as determined from the radiative balance at the top of the atmosphere and atmospheric transport calculations. The oceanic transport is obtained as a residual. [From Peixoto and Oort 1992, based on data from Carissimo *et al.* 1985]

both hemispheres (Figure 2). Less significant with respect to meridional heat transport is the relatively small basin of the Indian ocean. However, there is an interesting aspect in the Indian ocean in that the meridional heat transport shows a distinctly seasonal behavior due to the reversal of the Somali current crossing the equator from the north in February-March and in the opposite direction in fall. This is due to the strong monsoonal activity in this region.

Figure 2 already indicates the special role of the Atlantic ocean for meridional heat transport. At all latitudes the transport is directed northward with a maximum of about 1 PW at 30°N. A simple order-of-magnitude calculation shows that this heat transport cannot be due to the wind-driven surface circulation. At about 10°N surface currents in the Atlantic ocean are known to be relatively weak, but the northward heat transport is still about 1 PW. Taking a conservative estimate of a volume transport of about 20 Sv (1 Sv = 1 Sverdrup† = $10^6\text{m}^3/\text{s}$) of a weak anticyclonic gyre we require a west-east temperature difference of about

$$\Delta T = \frac{Q}{\rho c_p \dot{V}} \approx \frac{10^{15}\,\text{W}}{10^3\,\text{kg}\,\text{m}^{-3}\cdot 4\cdot 10^3\,\text{Jkg}^{-1}\text{K}^{-1}\cdot 20\cdot 10^6\,\text{m}^3\text{s}^{-1}} = 12\,\text{K}. \qquad (1)$$

This is in contrast with an observed annual mean temperature contrast between east and west of less than 2°C in the Atlantic at about 10°N. Therefore, there must be another type of circulation in the ocean that is much more efficient in carrying large amounts of heat. We will focus in the following sections on this circulation and demonstrate its prime importance for the dynamics in the climate system.

Apart from the capability of the ocean to transport large amounts of heat meridionally there

†**Sverdrup**, in the honour of *Harald U. Sverdrup* (1888–1957), theoretical oceanographer, director of Scripps Institution of Oceanography and author of one of the standard books in oceanography (Sverdrup *et al.* 1942), is a convenient unit for large-scale volume transport in the ocean. It was coined by the late *Max Dunbar* (1914–1995), Professor of Oceanography at McGill University. He told me that he also proposed the unit **Bering**, in the honour of *Vitus Bering* (1681–1741), a Danish explorer, who found that Asia and America were two separate continents and who charted the west coast of Alaska, 1 Be = $10^3\text{km}^3/\text{year}$; the latter is a common unit in the hydrological literature. The St. Lawrence River transports about 0.45 Be; global run-off is estimated at about 27 Be. The unit Bering, however, was never adopted.

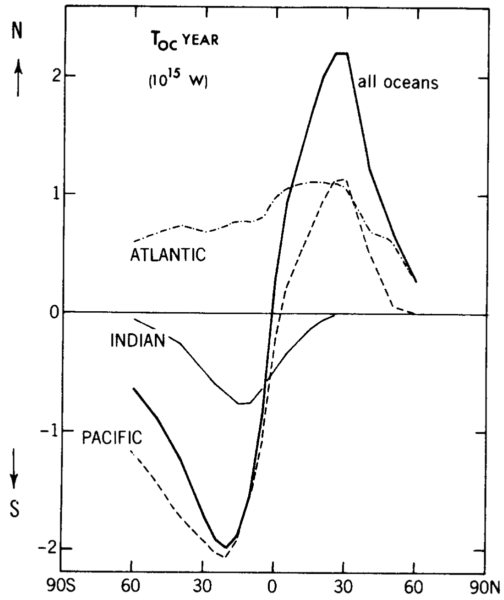

Figure 2: Annual mean meridional heat transport in the different ocean basins in units of PW (1 PW = 10^{15} W) determined from the divergence of the surface heat balance. [From Peixoto and Oort 1992, based on data from Hastenrath 1982]

are a number of feedback mechanisms associated with the surface buoyancy flux. The result is that the ocean has more than one stable equilibrium state under a given surface boundary condition. A review is given by Weaver and Hughes (1992) and this paper provides some more recent references in addition. Transitions between such states are fast and occur on typical time scales of a few decades. They are therefore prime candidates to explain rapid climatic shifts that have been observed and documented in many paleoclimatic archives (ice cores, tree rings, sea and lake sediments, etc.). Broecker and Denton (1989) give a review of these reconstructions.

2 Dynamics of Large-Scale Ocean Circulation

In this section we explain briefly the most important types of the large-scale ocean circulation and discuss their dynamics on an introductory level. The series of the Oceanography Course Team (1991) contains a broad but not very detailed introduction into various aspects of oceanography and Pickard and Emery (1990) focuses on the description of typical water masses and their transport paths. A good introduction of circulation theory is given in Pond and Pickard (1991) (ocean) and Gill (1982) (ocean and atmosphere); Warren and Wunsch (1981) gives an excellent review on the state-of-the art of physical oceanography at the time and Pedlosky (1987) is a more advanced and fairly mathematical text on fluid dynamics in a rotating frame. Pedlosky (1996) provides the most complete and profound presentation of theories of ocean circulation.

With large-scale we mean horizontal length scales that are typically of the order of a few 1000 km, i.e. they can cover entire ocean basins. To investigate the large-scale flow on a sphere, it is convenient to formulate the equations of motion on an f-plane or β-plane;

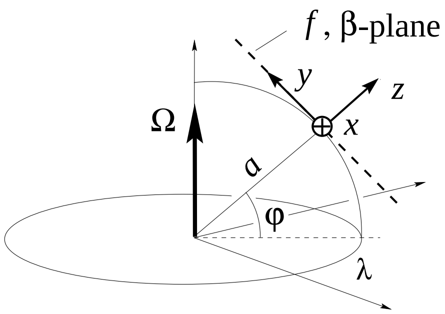

Figure 3: Geophysical coordinate system with f-plane or β-plane on which a local coordinate system (x, y, z) is defined. The coordinate system is rotating with angular velocity $\vec{\Omega}$ whose z-component is $\Omega \sin \varphi$.

spherical coordinates are approximated on a Cartesian coordinate system (x, y, z) whose origin is fixed at a given latitude φ (Figure 3).

The conservation of momentum for the two horizontal directions, neglecting non-linear terms, read,

$$\frac{\partial u}{\partial t} - f v = -\frac{1}{\rho}\frac{\partial p}{\partial x} + F_x \quad , \tag{2}$$

$$\frac{\partial v}{\partial t} + f u = -\frac{1}{\rho}\frac{\partial p}{\partial y} + F_y \quad , \tag{3}$$

where (u, v) are the eastward and northward velocity components, $f = 2\Omega \sin \varphi$ is the Coriolis parameter, ρ denotes density, p is pressure and Ω is the angular velocity of the Earth's rotation. F_x and F_y denote the horizontal components of friction, i.e. sources (e.g. wind) and sinks (e.g. frictional dissipation) of momentum at basin boundaries or in the interior.

The conservation equation of vertical momentum is simplified to the hydrostatic equilibrium

$$0 = -\frac{1}{\rho}\frac{\partial p}{\partial z} - g \quad . \tag{4}$$

Mass is conserved in the entire fluid, i.e.

$$\frac{\partial \rho}{\partial t} + \frac{\partial(\rho u)}{\partial x} + \frac{\partial(\rho v)}{\partial y} + \frac{\partial(\rho w)}{\partial z} = 0 \quad , \tag{5}$$

where w is the vertical component of velocity. An equation of state defines the density field from the fields of temperature and salinity. The density of sea water is dependent on temperature, salinity and pressure:

$$\rho = \rho(T, S, p) \approx \rho_0 \cdot \left(1 + \alpha \cdot (T - T_0) + \beta \cdot (S - S_0) + \gamma \cdot (T - T_0)^2\right) \quad , \tag{6}$$

where $T_0 = 0°\mathrm{C}$, $S_0 = 35\,\mathrm{psu}$, $\rho_0 = 1028.1\,\mathrm{kg/m^3}$, $\alpha = -5.26 \cdot 10^{-5}\,\mathrm{K^{-1}}$, $\beta = 7.86 \cdot 10^{-4}\,\mathrm{psu^{-1}}$ and $\gamma = -6.6 \cdot 10^{-6}\,\mathrm{K^{-2}}$, see Gill (1982) and Pierce *et al.* (1995). Equation 6 is an approximation to the fully pressure-dependent UNESCO equation of state (Gill 1982; Wright 1996). It is important to note that there is a non-linear term in (6) which is responsible for the fact that density variations due to salinity changes are stronger at lower temperature. This can lead to mixing instabilities in that the mixture of two water parcels with (T_1, S_1) and (T_2, S_2)

	inertial $\partial/\partial t$	Coriolis fu, fv	pressure gradient ∇p	forcing	dissipation
				F_x, F_y	
geostrophic	–	$\surd$	$\surd$	–	–
Ekman	–	$\surd$	–	$\surd$	$\surd$
Sverdrup	–	$\surd$	$\surd$	$\surd$	–
Stommel	–	$\surd$	$\surd$	$\surd$	$\surd$

Table 1: Depending on the terms which balance in the momentum equations 2 and 3 specific flow regimes develop. The balancing terms are marked by $\surd$.

is denser than each of the components: $\rho\left(\frac{1}{2}(T_1+T_2), \frac{1}{2}(S_1+S_2)\right) > \frac{1}{2}\rho(T_1,S_1)+\frac{1}{2}\rho(T_2,S_2)$. Such mixing instabilities are called "cabbeling" (or caballing) and indications have been found in high latitude waters (Foster and Carmack 1976; Carmack 1986).

Finally, conservation equations for temperature (energy) and salinity have to be formulated:

$$\frac{\partial T}{\partial t} + u\frac{\partial T}{\partial x} + v\frac{\partial T}{\partial y} + w\frac{\partial T}{\partial z} = K_x\frac{\partial^2 T}{\partial x^2} + K_y\frac{\partial^2 T}{\partial y^2} + K_z\frac{\partial^2 T}{\partial z^2} + Q_T \quad , \tag{7}$$

$$\frac{\partial S}{\partial t} + u\frac{\partial S}{\partial x} + v\frac{\partial S}{\partial y} + w\frac{\partial S}{\partial z} = K_x\frac{\partial^2 S}{\partial x^2} + K_y\frac{\partial^2 S}{\partial y^2} + K_z\frac{\partial^2 S}{\partial z^2} + Q_S \quad , \tag{8}$$

where K_x, K_y and K_z are constant eddy diffusivities and Q_T and Q_S denote sources–sinks of temperature and salinity, respectively. They are due to diabatic heating or convective events or to atmosphere-ocean surface fluxes. Diffusion processes in (7) and (8) are crude approximations to the real mixing processes. Mixing in the ocean, and in any real fluid, is due to smaller-scale circulations, eddies and, eventually turbulent motion. The above parameterisation based on lateral eddy-diffusivity is the simplest possible formulation. Recent development of better schemes taking into account that water parcels move along isopycnals (surfaces of constant density) exihibit better agreement with observations. A first approach was proposed by Redi (1982) and more recent theoretical work also accounts for the effect of baroclinic eddies on the density field (Gent and McWilliams 1990; Gent *et al.* 1995) with promising results in the ocean general circulation models (Danabasoglu *et al.* 1994).

The seven equations (2)–(8) determine, with suitable boundary conditions, the seven unknowns u, v, w, p, ρ, T and S. We now discuss successive approximations to the equations presented above according to Table 1. We restrict the discussion here on stationary flows and thus ignore the inertial terms. This implies that we consider time scales longer than typically a few years.

2.1 Geostrophic Flow

The simplest possible, non-trivial solution of the momentum equations (2) and (3) is the geostrophic balance, i.e. the balance between Coriolis forces and pressure gradient forces. In the northern hemisphere, the flow is (counter-) clockwise about a center of (low) high pressure (Pond and Pickard 1991). Away from boundaries and also in the deep interior ocean, the geostrophic balance is a fair approximation of the time-mean flow. Given the hydrography ($T(p)$, and $S(p)$) of a section, it is straightforward to calculate relative geostrophic velocities. However, to determine absolute velocities and transports one needs to know a level of reference, i.e. the absolute velocity has to be known at one level. Surface and

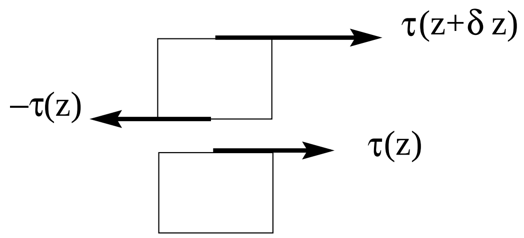

Figure 4: Illustration of the surface stresses and the resulting acceleration per unit mass due to friction between two adjacent fluid elements.

bottom are not good locations since the effect of friction disturbs the geostrophic balance significantly. Often, an arbitrary level of 2000 m is assumed to be the 'level of no motion', but there are more dynamical methods to determine this (Stommel and Schott 1977).

2.2 Ekman Flow

Close to basin boundaries such as the bottom or the surface or lateral boundaries, the effect of friction is important. It is the principal mechanism of dissipation of momentum input into the ocean by the wind at the surface. The presence of this effect is estimated by a non-dimensional number, the Ekman number, which is the ratio between frictional and Coriolis acceleration,

$$E = \frac{\text{frictional acceleration}}{\text{Coriolis acceleration}} = \frac{AU/L^2}{fU} \quad , \tag{9}$$

where A is an eddy viscosity, U is a velocity scale and L is a length scale. If $E = o(1)$, frictional effects cannot be neglected. Close to the ocean surface the vertical eddy viscosity A_z is order $10^{-1}\,\mathrm{m^2/s}$, $f \approx 10^{-4}\,\mathrm{s^{-1}}$ and $L \approx 10^2\mathrm{m}$ which yields $E \approx 0.1$ (Pond and Pickard 1991). Therefore, the Ekman flow is important in the top few tens to hundred meters of the ocean.

We now assume that the velocity field can be separated into a large-scale geostrophic part (u_g, v_g) and a part that takes into account the processes of friction, (u_E, v_E). Upon neglecting the inertial terms we can write eq. 2 and 3,

$$-fv_g - fv_E = -\frac{1}{\rho}\frac{\partial p}{\partial x} + F_x \quad , \tag{10}$$

$$fu_g + fu_E = -\frac{1}{\rho}\frac{\partial p}{\partial y} + F_y \quad . \tag{11}$$

The frictional forces must now be determined. We assume an inviscid fluid, i.e. fluxes of momentum in the interior of the fluid are neglected. The resulting body force per unit mass, F_x, on a fluid element due to horizontal stresses τ onn its surfaces (see Figure 4) is given by

$$F_x \cdot \rho\delta x\delta y\delta z = (\tau(z+\delta z) - \tau(z)) \cdot \delta x\delta y \quad , \tag{12}$$

and hence,

$$F_x = \frac{1}{\rho}\frac{\partial \tau_x}{\partial z}, \quad F_y = \frac{1}{\rho}\frac{\partial \tau_y}{\partial z} \quad . \tag{13}$$

Introducing (13) into (10) and (11), and assuming geostrophic balance for u_g and v_g we obtain, upon integrating from a depth $z = -h$ to the surface $z = 0$,

$$-f \int_{-h}^{0} \rho v_E \, dz = \tau_x(0) - \tau_x(-h) \quad , \tag{14}$$

$$f \int_{-h}^{0} \rho u_E \, dz = \tau_y(0) - \tau_y(-h) \quad . \tag{15}$$

Stresses at the ocean surface are due to wind action while interior stresses at a depth $-h$, (a few tens to hundred meters) are much smaller and will be neglected for the surface Ekman layer. The opposite is true for bottom Ekman layers. We now define the horizontal mass flux vector $\mathbf{M}$ according to

$$\mathbf{M} = (M_x, M_y, 0) = \left(\int_{-h}^{0} \rho u \, dz, \int_{-h}^{0} \rho v \, dz, 0 \right) \quad , \tag{16}$$

and recast (14) and (15) in vector notation:

$$\mathbf{M_E} = -\frac{1}{f} (\mathbf{k} \times \boldsymbol{\tau}) \quad , \tag{17}$$

where $\mathbf{k}$ is a unit vector in the z-direction, and $\boldsymbol{\tau}$ denotes the surface wind stress vector. The depth-integrated Ekman mass transport is directed 90° to the right (left) with respect to the direction of the wind stress on the northern (southern) hemisphere. The transport is increasing towards the equator due to the decrease of the Coriolis parameter.

Equation 17 has important implications, especially at continental boundaries and at the equator. One example of the former are northward winds along the Peruvian coast. These winds generate an Ekman transport $M_{Ex} < 0$ away from the coast. Due to mass continuity this mass must be supplied from below which leads to intensive coastal upwelling in that region. This keeps the sea surface temperatures about 7°C colder than a typical zonal average for that latitude as long as wind stress is present. During El Niño conditions this wind stress is greatly reduced resulting in a relaxation of the upwelling and a large warming of the near-surface layers waters follows (Philander 1990). Across the equator the sign of f changes and for a spatially constant wind stress τ, $\mathbf{M_E}$ has an antisymmetric singularity at the equator. Integrating the continuity equation meridionally in a narrow band across the equator leads to equatorial upwelling.

Taking now the divergence of (17) and recognizing that

$$\int_{-h}^{0} \left(\frac{\partial \rho u}{\partial x} + \frac{\partial \rho v}{\partial y} \right) dz + \rho w(0) - \rho w(-h) = \nabla \cdot \mathbf{M} + \rho w(0) - \rho w(-h) = 0 \quad , \tag{18}$$

we obtain for the vertical velocity at the base of the Ekman layer

$$w(-h) = \frac{1}{\rho} \mathbf{k} \cdot \left(\nabla \times \frac{\boldsymbol{\tau}}{f} \right) \quad , \tag{19}$$

where we have used the rigid-lid approximation $w(0) = 0$. Eq. 19 implies that the curl of the wind stress induces vertical velocities at the base of the Ekman layer. We have also assumed that the density of the Ekman layer is uniform.

Assume now an f-plane and a zonal wind stress that increases with latitude, $\partial\tau_x/\partial y > 0$ which leads to downwelling, $w(-h) < 0$; this is called *Ekman pumping*, the opposite effect is referred to as *Ekman suction* in the *northern* hemisphere where $f > 0$. The opposite is true in the southern hemisphere. Upwelling tends to bow isopycnals (lines of constant density) upwards, a feature which indeed is observed in the ocean. Slopes of isopycnals cause horizontal pressure gradients which, themselves, can drive geostrophic flow. This makes clear that Ekman flow has important implications and can generate large-scale flow through interior processes in a stratified fluid.

2.3 Sverdrup Balance

The Sverdrup balance is a powerful diagnostic means to obtain a first estimate of the depth-integrated, large-scale mass transport that results from a given surface wind stress. One considers the balance of wind stress, Coriolis and pressure gradient forces. We assume a β-plane, i.e. we take a Taylor expansion of the Coriolis parameter around the latitude φ_0,

$$f(\varphi) \approx f_0 + \frac{1}{a}\frac{\partial f}{\partial\varphi}\bigg|_{\varphi_0}(y - y_0) \quad , \tag{20}$$

where $f_0 = 2\Omega\sin\varphi_0$ and define

$$\beta \equiv \frac{1}{a}\frac{\partial f}{\partial\varphi}\bigg|_{\varphi_0} = \frac{2\Omega\cos\varphi_0}{a} \quad , \tag{21}$$

where a is the Earth's radius and $y_0 = a \cdot \varphi_0$. Balancing the Coriolis, pressure gradient and friction terms, the momentum equations (2) and (3) read, upon integration from the bottom $z = -H$ of a flat basin to the surface

$$-fM_y = -\int_{-H}^{0}\frac{\partial p}{\partial x}\,dz + \tau_x(0) \quad , \tag{22}$$

$$fM_x = -\int_{-H}^{0}\frac{\partial p}{\partial y}\,dz + \tau_y(0) \quad , \tag{23}$$

where the bottom stress has been neglected. By differentiating (22) by y and (23) by x and taking the difference, we obtain

$$\beta M_y = \mathbf{k}\cdot(\nabla\times\boldsymbol{\tau}) \quad . \tag{24}$$

We have used (18) and $w(0) = w(-H) = 0$ at the surface and the bottom of the basin. Eq. 24 is the Sverdrup balance and is valid in regions where frictional dissipation can be neglected. Note that this transport is due to the β-effect, i.e. the spherical shape of the Earth. We will see below that this flow can also be understood in terms of the conservation of potential vorticity. The Sverdrup balance has been used to chart the depth-integrated volume transport of the major ocean basins (Reid 1994).

Take a typical situation in the middle latitudes in the transition zone between the easterly and the westerly winds (Fig. 5). The meridional wind stress component is much smaller than the zonal, whose derivative is positive in the y-direction. Therefore, the Sverdrup transport is directed to the south at all latitudes of the region in consideration. The Sverdrup balance, however, is not a solution of the closed basin. This indicates that important processes have been neglected and further analysis is required.

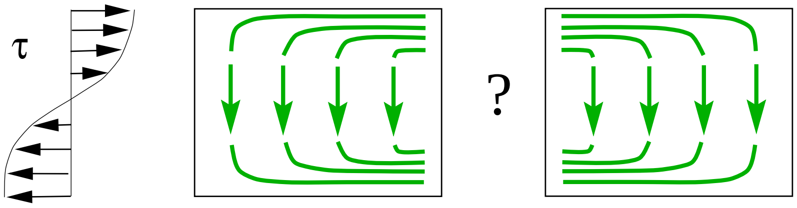

Figure 5: A typical mid-latitude zonal wind stress τ causes a depth-integrated flow that is directed southward. The Sverdrup balance is not a solution of the closed basin and does not resolve the question whether the flow develops an eastern or a western boundary current or whether the flow will be east-west symmetric.

2.4 Western Boundary Currents

The problem of the large-scale circulation in a closed basin is now addressed. Judging from the wind stress one would argue that the flow should be directed towards the east in the northern half of the basin and towards the west in the southern half of the basin (Fig. 5, right). Moreover, Ekman theory implies that this wind stress produces Ekman convergence along the central latitude of the basin. This elevates the sea surface and lowers isopycnals in the interior resulting in an anticyclonic geostrophic flow. However, it is not clear at all whether such a flow will be east-west symmetric or whether there will be an intense current along one or both coast lines.

The Gulf stream has been utilized by travelers and known to oceanographers for centuries, and it was one of the grand challenges of early physical oceanography to formulate a theory that explains why such strong currents develop and do so preferentially at eastern continental boundaries (i.e. western boundaries with respect to the ocean basin). Examples are the Gulf and Kuroshio streams and the Brazil current. A historical review and excellent treatise of Gulf Stream theories is given by Stommel (1965).

After many decades of fruitless attempts and qualitative explanations of the "western intensification" the simple model developed by Henry Stommel was a break-through (Stommel 1948). The model beautifully demonstrates in the simplest possible setting that western intensification is the result of wind stress acting on a fluid on a rotating sphere.

The original model considers a near-surface, vertically uniform layer (200 m deep) in a rectangular basin of extent $0 < x < L$ and $0 < y < M$ and assumes that there is no vertical mass flux across the basal interface. Momentum that is generated at the surface by wind stress is dissipated at the lower interface. The simplest possible parameterization of Rayleigh friction is used, i.e.

$$F_x = \frac{1}{\rho}\frac{\partial \tau_x}{\partial z} - Ru \quad , \tag{25}$$

$$F_y = \frac{1}{\rho}\frac{\partial \tau_y}{\partial z} - Rv \quad , \tag{26}$$

where $R\mathbf{v}$ is a body force acting throughout this layer and representing the effect of momentum dissipation. The friction coefficient R is an inverse spin-down time of about 1/11 days.

Performing the same operations as for the derivation of the Sverdrup balance we obtain

$$-\beta M_y = \frac{\partial \tau_x(0)}{\partial y} - \frac{\partial \tau_y(0)}{\partial x} + R\left(\frac{\partial M_y}{\partial x} - \frac{\partial M_x}{\partial y}\right) \quad . \tag{27}$$

According to the above assumptions, mass is conserved in the slab and we can define a mass transport streamfunction Ψ given by

$$M_x = -\frac{\partial \Psi}{\partial y}, \quad M_y = \frac{\partial \Psi}{\partial x} \quad . \tag{28}$$

Introducing (28) into (27) we obtain

$$-\beta \frac{\partial \Psi}{\partial x} = \frac{\partial \tau_x}{\partial y} - \frac{\partial \tau_y}{\partial x} + R\left(\frac{\partial^2 \Psi}{\partial x^2} + \frac{\partial^2 \Psi}{\partial y^2}\right) \quad , \tag{29}$$

where τ_x and τ_y are the wind stress components at the sea surface. This linear partial differential equation must be supplemented by boundary conditions: no mass flux through the lateral boundaries implies $\Psi = const$ on this boundary. Since only derivatives of Ψ occur in (29) we can set $\Psi = 0$ on the boundary.

Stommel selected a purely zonal wind stress profile given by

$$\tau_y = 0, \quad \tau_x = -T\cos\left(\frac{\pi y}{M}\right) \quad . \tag{30}$$

Separation of the variables using

$$\Psi(x, y) = \psi(x) \cdot \sin\left(\frac{\pi y}{M}\right) \quad , \tag{31}$$

yields the following ordinary differential equation in ψ:

$$R\frac{d^2\psi}{dx^2} + \beta\frac{d\psi}{dx} - R\left(\frac{\pi}{M}\right)^2 \psi = -\frac{T\pi}{M} \quad , \tag{32}$$

with the boundary conditions

$$\psi(0) = 0 \quad , \quad \psi(L) = 0 \quad . \tag{33}$$

Before solving (32) we consider two special cases. First, if there is no friction, $R = 0$, we can integrate (32). Satisfying only one boundary condition at the eastern boundary $x = L$, we obtain

$$\psi(x) = \frac{T\pi}{\beta M}(L - x) \quad . \tag{34}$$

This is the Sverdrup balance. It is, however, not a permissible solution of the closed basin since $\psi(0) \neq 0$.

Second, we assume a rotating flat Earth where $\beta = 0$. A solution of (32) satisfying both boundary conditions reads

$$\psi(x) = \frac{TM}{R\pi}\left(1 - \frac{\sinh(\pi(L - x)/M) + \sinh(\pi x/M)}{\sinh(\pi L/M)}\right) \quad . \tag{35}$$

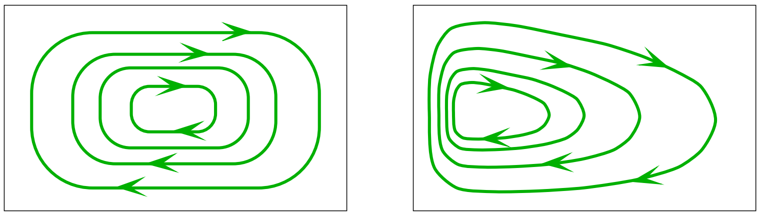

Figure 6: Scetch of streamlines of the wind driven circulation with Rayleigh friction (Stommel 1948). Only in the case of a latitudinal dependence of the Coriolis parameter is there a western intensification of the flow. Away from the western boundary, the flow is directed southward everywhere and in near Sverdrup balance.

This solution is symmetric about $x = \frac{1}{2}L$ and hence uniform rotation alone cannot be the cause of western intensification either (Fig. 6, left).

The complete solution, satisfying $\Psi = 0$ on the boundaries is given by

$$\Psi(x,y) = \frac{TM}{R\pi}\left(1 - \frac{(1-\mathrm{e}^{D_2L})\mathrm{e}^{D_1x} - (1-\mathrm{e}^{D_1L})\mathrm{e}^{D_2x}}{\mathrm{e}^{D_1L} - \mathrm{e}^{D_2L}}\right)\sin\left(\frac{\pi y}{M}\right) \quad , \tag{36}$$

where

$$\left.\begin{matrix} D_1 \\ D_2 \end{matrix}\right\} = -\frac{\beta}{2R} \pm \sqrt{\left(\frac{\beta}{2R}\right)^2 + \left(\frac{\pi}{M}\right)^2} \quad . \tag{37}$$

A typical length scale $\delta = R/\beta$ emerges in solution (36). It is the width of the western boundary layer, estimated at

$$\delta = \frac{R}{\beta} \approx \frac{10^{-6}\mathrm{s}^{-1}}{2\cdot 10^{-11}\mathrm{m}^{-1}\mathrm{s}^{-1}} \approx 50\,\mathrm{km} \quad , \tag{38}$$

and called *Stommel layer* (see Fig. 6, right). A series of other models of the wind driven circulation has been proposed with different parameterizations of dissipation of the input of momentum due to the wind stress (for a summary and references see Veronis (1981)). Depending on these parameterizations, different boundary layer thicknesses and circulation patterns adjacent to the western boundary result.

2.5 Deep Circulation

For a deep ocean in approximate diffusive equilibrium one would expect the deep ocean temperature to assume values that are close to the global mean of sea surface temperature. However, early measurements and, first global surveys performed in the thirties by Wüst (1935) – the most recent data sets are compiled by Levitus (1982) and Levitus and Boyer (1994) – clearly demonstrate that the deep ocean is cold and the coldest waters in the deep ocean derive from localized regions in the northern and southern high latitudes (Stommel 1962). Therefore, a steady supply of such cold water must feed the deep ocean. Mass continuity requires that this water must eventually upwell, a process for which there is no evidence that it occurs in specific, small regions. In contrast to the deep water formation, upwelling from deep is a basin-scale feature, hence the vertical velocities are rather small. Based on a combination of radiocarbon and T and S measurements in the Pacific, Munk

(1966) estimated basin-mean values of the upwelling velocity and the vertical diffusivity. He obtained the canonical values

$$K_V = 1.3 \cdot 10^{-4}\,\mathrm{m}^2/\mathrm{s}\ , \quad w = 4.4\,\mathrm{m/yr} \quad . \tag{39}$$

Based on w we can estimate the minimum global deep water formation rate and obtain

$$\dot{V} = w \cdot A \approx 1.57 \cdot 10^{15}\,\mathrm{m}^3/\mathrm{yr} = 50 \cdot 10^6\,\mathrm{m}^3/\mathrm{s} = 50\,\mathrm{Sv} \quad , \tag{40}$$

where $A = 3.57 \cdot 10^{14}\mathrm{m}^2$ is an approximation of the global ocean surface. A census of the ocean water, based on T and S, reveals that the deep water derives primarily from two source regions: the Norwegian-Greenland-Iceland Sea and the Weddell Sea (Warren 1981).

The model of Stommel (1958), Stommel and Arons (1960a) and Stommel and Arons (1960b) is intuitively based on these observations. To derive the basic mechanism of the steady-state circulation, a sectorial slab of thickness H and uniform density ρ in the ocean interior is located on a rotating sphere. The flow field in the slab is assumed to have no vertical dependence, i.e. we only consider the depth-integrated mean. The flow is driven by broad upwelling which is uniform over the upper interface of the slab. For example, we choose 1000 m as the depth of the upper interface and assume a flat bottom at 4000 m. In spherical coordinates (Fig. 3) the geostrophic balance reads

$$-2\Omega \sin\varphi \cdot v = -\frac{g}{a\cos\varphi}\frac{\partial\eta}{\partial\lambda} \quad , \tag{41}$$

$$2\Omega \sin\varphi \cdot u = -\frac{g}{a}\frac{\partial\eta}{\partial\varphi} \quad , \tag{42}$$

where η is an elevation of the upper interface at 1000 m. The geostrophic balance is supplemented by a mass continuity equation. In the case of uniform density ρ, the mass balance is equivalent to the volume balance times a factor ρ. Therefore, the volume balance of of a volume element in spherical coordinates (Fig. 7) is given by

$$Hv_1 a\cos\varphi_1\delta\lambda - Hv_2 a\cos\varphi_2\delta\lambda + Hu_1 a\delta\varphi - Hu_2 a\delta\varphi - Qa^2\cos\varphi\delta\varphi\delta\lambda = 0 \tag{43}$$

where the last term of the l.h.s. denotes the continuous loss of volume (mass) by upwelling through the upper interface with a flux rate Q in $\mathrm{m}^3/(\mathrm{s}\cdot\mathrm{m}^2)$. The differential form of (43) is thus given by

$$\frac{\partial(v\cos\varphi)}{\partial\varphi} + \frac{\partial u}{\partial\lambda} + \frac{Qa}{H}\cos\varphi = 0 \quad . \tag{44}$$

The volume (mass) lost from this slab to the upper ocean must be supplied by deep water formation in a small region at high latitudes. Let S_0 denote this deep water formation rate (in m^3/s).

By cross-differentiating (41) and (42) the pressure gradient terms can be eliminated and we get an expression for the meridional velocity component v. Using (44) and integrating zonally from the eastern boundary (where $u = 0$) towards the west we also obtain an expression of the zonal velocity u. The two velocity components are given by

$$v = \frac{Qa}{H}\tan\varphi\ , \quad u = \frac{2Qa}{H}(\Lambda_1 - \lambda)\cos\varphi \quad , \tag{45}$$

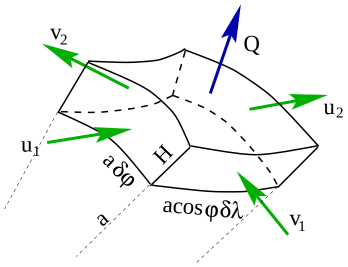

Figure 7: Volume element in spherical coordinates to derive the continuity equation.

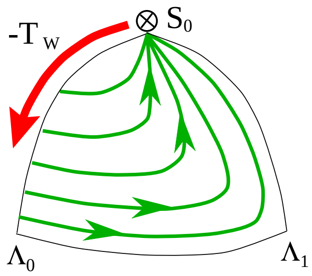

Figure 8: The geostrophic flow in the interior of a sectorial deep basin is directed polewards at all latitudes. Deep water is formed at the rate S_0 and a deep western boundary current is flowing southward feeding the flow in the interior.

where we have assumed that the sectorial ocean basin is between western and eastern longitudes Λ_0 and Λ_1, respectively and extending to the pole. A fundamental but counter-intuitive result of this analysis is the fact that $v > 0$ in the northern hemisphere. Therefore, the interior deep geostrophic flow is directed poleward at all latitudes; note that this result is independent of *where* the source S_0 is located. If the source S_0 of deep water is in the high northern latitude, as is the case in reality (see Dickson and Brown (1994) for a review), this leads to the conclusion that the deep water flows *towards* its source (Fig. 8). This is surprising, at first, since one would expect that water flows *away* from a source area. However, we will see that this, again, is a consequence of the conservation of potential vorticity in the deep layer and therefore due to the β-effect.

The mass that is lost through the upper interface must be supplied from somewhere. The zonal velocity u is directed eastward and hence emanates from the western boundary from which this mass is fed into the interior. The model of Stommel (1958) therefore *requires* a deep western boundary current.

There was circumstantial evidence from observations and geostrophic calculations (Defant 1941) already before the formulation of a dynamical theory. However, direct measurements of the deep western boundary current were first achieved by Swallow and Worthington (1957) using buoyant floats.

The zonally integrated meridional volume transport in the interior of the basin across latitude φ is denoted by $T(\varphi)$ and given by

$$T(\varphi) = \int_{\Lambda_0}^{\Lambda_1} d\lambda a \cos\varphi H v = Q a^2 (\Lambda_1 - \Lambda_0) \sin\varphi \quad , \tag{46}$$

where we have used (45). The transport in the western boundary current, $T_W(\varphi)$, can now be calculated as a residual. Balance of volume (mass) of the sector shown in Fig. 8 extending from latitude φ to the pole reads:

$$T_W(\varphi) + T(\varphi) + S_0 - Q \int_{\Lambda_0}^{\Lambda_1} d\lambda a \int_{\varphi}^{\pi/2} d\varphi a \cos\varphi = 0 \quad , \tag{47}$$

and hence

$$T_W(\varphi) = -S_0 - Qa^2(\Lambda_1 - \Lambda_0)(2\sin\varphi - 1) \quad , \tag{48}$$

where S_0 is the volume flux due to the source of new deep water localized at the pole as in Fig. 8. Equations (45) and (48) contain the following fundamental results of the model of Stommel and Arons (1960a) and Stommel and Arons (1960b):

1. the existence of a deep western boundary current (DWBC);
2. in the interior, where the geostrophic balance is valid, the water is recirculating towards the source S_0;
3. this recirculation is driven by uniform upwelling;
4. close to the source S_0 of newly formed deep water the deep boundary current is stronger than S_0 due to the recirculation;
5. there is no transport across the equator in the interior.

For simplicity consider now a closed basin that extends from the equator ($\varphi = 0$) to the pole (Fig. 8). In this case, all the new deep water must upwell, i.e. $S_0 = Qa^2(\Lambda_1 - \Lambda_0)$ and (48) simplifies to

$$T_W(\varphi) = -2S_0 \sin\varphi \quad . \tag{49}$$

Close to the source region ($\varphi \to \pi/2$), the flow rate of the western boundary current is twice that of the source of newly formed deep water! The current then "bleeds out" towards the south because it feeds the geostrophic interior. In the above case, the DWBC vanishes at the equator, but it is obvious from (48) that water can cross the equator in the DWBC provided $S_0 > Qa^2(\Lambda_1 - \Lambda_0)$.

The Stommel model is stationary. Kawase (1987) has investigated the time dependent problem and found the dynamical explanation for the development of a deep western boundary current feeding into an adjacent interior. The choice of a uniform and constant vertical velocity w must then be replaced by a parameterization connecting it to the interior flow. The selection $w = -K \cdot \eta$ with a damping constant K, states that the upwelling tends to restore the interface elevation η. In the limit of weak damping, the equilibrium state of the model is identical with the Stommel-Arons model. A mass source in the north-western corner of a sectorial basin, symmetric to the equator, is switched on and its evolution depending on K is studied. The mass source initiates a Kelvin wave that leads the developing DWBC and travels south along the western boundary, then propagates eastward along the equator and poleward along the eastern boundaries. For strong damping the DWBC does not cross the equator but follows it eastward and leaks into both hemispheres. Kawase (1987) could show that for weak damping the Kelvin wave transports enough energy that long Rossby waves can be generated at the eastern boundary. These Rossby waves then radiate into the interior and set up the typical interior flow pattern found by Stommel and Arons (1960a).

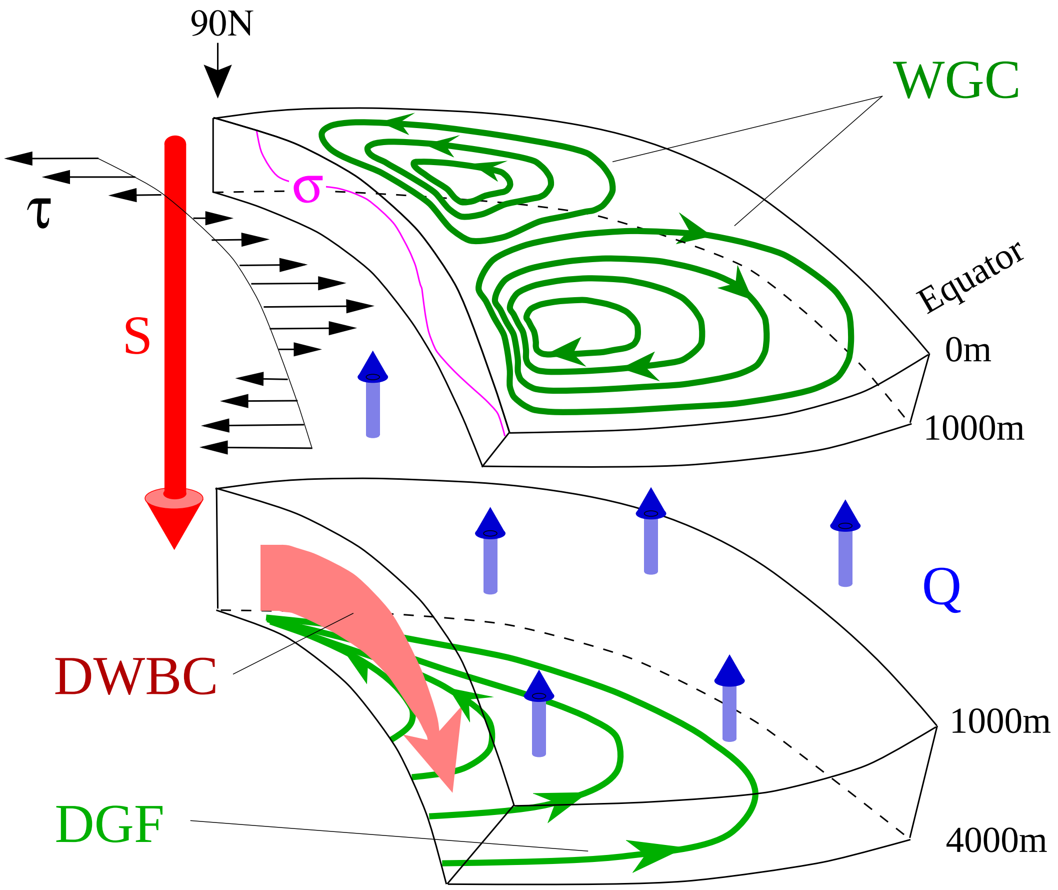

Figure 9: Schematic view of the different types of steady-state circulations in a sectorial ocean basin extending from the equator to the pole with a longitudinal extent of roughly 60°. Wind stress τ drives a *wind driven gyre circulation* (WGC) which shows western intensification due to the β-effect. τ also causes Ekman suction in the northerly and Ekman pumping in the southerly upper layer giving a near-surface isopycnal surface σ its typical shape: the isopycnal is shallow below the subpolar gyre and deep below the subtropical gyre. A source of newly formed deep water, S_0, feeds the deep ocean in which a *deep western boundary current* (DWBC) develops from which the *deep geostrophic flow* (DGF) of the interior is derived. DGF flows northward to conserve potential vorticity while slowly upwelling. This results in a vertical mass flux Q that closes the flow. In reality, $Q < S_0$ in this sector and the DWBC is crossing the equator setting up a global circulation (Stommel 1958; Broecker 1991).

2.6 A Panoramic View of the General Circulation

a) Summary

We can now combine the four major circulation types of Table 1 into a single view of how the circulation in a basin operates on large spatial scales. This attempt is made in Figure 9. The general circulation is forced by the input of momentum through surface wind stress τ and by the flux of buoyancy, indicated by the vertical arrow S_0 and uniform upwelling Q. The surface wind stress forces the wind-driven geostrophic circulation (WGC) which is intensified at the western boundary and forms the subtropical and the subpolar gyres. Ekman pumping and Ekman suction change the local depth of the near-surface isopycnals σ which set up horizontal pressure gradients with associated geostrophic flows. They are responsible for the fact that the wind driven gyres do not extend all the way to the bottom

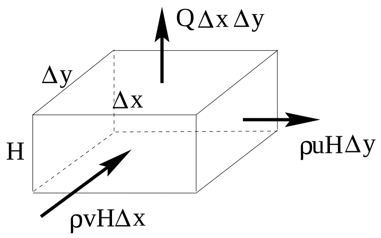

Figure 10: Control volume $\delta x \cdot \delta y \cdot H$ embedded in a fluid of constant density ρ. The horizontal velocity field (u, v) and the net vertical mass flux Q lead to changes of the height H of the control volume.

but are compensated by sloping isopycnals in the top few hundred meters. In other words, the geostrophic velocities exhibit a vertical structure ("thermal wind", see Pond and Pickard (1991)).

The source S_0 feeds the deep western boundary current (DWBC) which flows southward and leaks into the deep interior where the geostrophic flow (DGF) is directed polewards at all latitudes. The DGF recirculates into the source area the DWBC whose initial strength is $2 \times S_0$. There is a cross-interface mass flux Q into the upper 1000 m which supplies the mass lost due to S_0 in the upper layer.

b) Conservation of Potential Vorticity

A deeper understanding of geophysical flow is reached by considering a quantity that accounts for the conservation of angular momentum (Pedlosky 1987; Pond and Pickard 1991). The horizontal momentum equations read

$$\frac{Du}{Dt} - fv = -\frac{1}{\rho}\frac{\partial p}{\partial x} + F_x \quad , \tag{50}$$

$$\frac{Dv}{Dt} + fu = -\frac{1}{\rho}\frac{\partial p}{\partial y} + F_y \quad , \tag{51}$$

where the material derivative has been used:

$$\frac{D}{Dt} \equiv \frac{\partial}{\partial t} + u\frac{\partial}{\partial x} + v\frac{\partial}{\partial y} \ . \tag{52}$$

Cross-differentiating the horizontal momentum equations the pressure terms are eliminated. With the definition of the relative vorticity ζ

$$\zeta = \frac{\partial v}{\partial x} - \frac{\partial u}{\partial y} \quad , \tag{53}$$

we obtain, assuming $\rho = const$,

$$\frac{D}{Dt}(\zeta + f) = -(\zeta + f)\left(\frac{\partial u}{\partial x} + \frac{\partial v}{\partial y}\right) + \frac{\partial F_y}{\partial x} - \frac{\partial F_x}{\partial y} \quad , \tag{54}$$

We now turn to the balance of mass. Consider a control volume $\delta x \cdot \delta y \cdot H$ embedded in a fluid (Fig. 10) of constant ρ whose horizontal velocity field is given by (u, v). Vertical motion is accounted for by Q, the net vertical mass flux per unit area out of the control volume (positive Q means mass loss of the control volume, i.e. upward motion). The balance of mass in the control volume reads

$$\frac{\partial}{\partial t}(\rho\Delta x\Delta yH) = \rho uH\Delta y|_x - \rho uH\Delta y|_{x+\Delta x}\,\rho vH\Delta x|_y - \rho vH\Delta x|_{y+\Delta y} - Q\Delta x\Delta y \quad , \tag{55}$$

which, in the limit of $(\Delta x, \Delta y) \to 0$, results in

$$\frac{\partial}{\partial t}(\rho H) = -\frac{\partial}{\partial x}(\rho Hu) - \frac{\partial}{\partial y}(\rho Hv) - Q\ . \tag{56}$$

Dividing (eq. 56) by ρ and using (eq. 52) we obtain

$$\frac{1}{H}\frac{DH}{Dt} + \left(\frac{\partial u}{\partial x} + \frac{\partial v}{\partial y}\right) = -\frac{Q}{\rho H} \quad . \tag{57}$$

Combining (54) with (57) we arrive at the conservation equation of potential vorticity

$$\frac{D}{Dt}\left(\frac{\zeta + f}{H}\right) = \left(\frac{\zeta + f}{H}\right)\frac{Q}{\rho H} + \frac{1}{H}\left(\frac{\partial F_y}{\partial x} - \frac{\partial F_x}{\partial y}\right) \quad . \tag{58}$$

We note from (58) that, following the fluid element, potential vorticity is generated (or dissipated) by mass fluxes and friction. This concept is important, for example, for the flow between adjacent isopycnal surfaces. Mixing across isopycnals is strongly reduced since energy must be available to achieve this mixing. Therefore, isopycnals are good models of material surfaces through which there is no mass flux. On an interior isopycnal, away from Ekman layers, potential vorticity is thus a nearly conserved quantity. We conclude from (58) that if a fluid column of constant depth H moves northward, f increases and ζ must decrease and hence turns clockwise (this is the familiar effect of the Coriolis force). If it moves zonally, $f = const$ and the relative vorticity remains constant, too. On large scales $\zeta \ll f$ (see below) and hence a southward flowing fluid column will be compressed, i.e. H decreases. As a consequence, we observe near-surface isopycnals in the eastern, low-latitude Atlantic that shallow towards the south.

The wind driven circulation and the deep circulation are now discussed in the framework of the conservation of potential vorticity. In the case of the wind driven circulation, Stommel considered a system where mass was not exchanged vertically, i.e. $Q = 0$, and potential vorticity is generated by wind stress and dissipated by Rayleigh friction or eddies. An estimate of the scales involved suggests that the relative vorticity ζ can be neglected against the planetary vorticity f in this discussion:

$$\frac{\zeta}{f} \approx \frac{U}{fL} \approx \frac{0.1\,\mathrm{m\,s^{-1}}}{10^{-4}\,\mathrm{s^{-1}}\cdot 10^{6}\,\mathrm{m}} = 10^{-3} \quad . \tag{59}$$

Wind stress in our example (eq. 30) inputs negative vorticity into the ocean and hence tends to reduce potential vorticity. Table 2 shows the possible vorticity balances for meridional flow. Note that zonal flow does not change the planetary vorticity since $f = const.$

In the southward flow in the Sverdrup interior, $\partial v/\partial x$ is small and the input of negative vorticity by wind stress is balanced by the gain of negative vorticity due to southward motion (reduction of planetary vorticity). In the northward flow, however, vorticity balance is only achieved if the current has a strong shear. The gain of vorticity that is required if the fluid

Current	$\dfrac{D\zeta}{Dt}$	$\dfrac{Df}{Dt}$	$\dfrac{\partial\tau_y}{\partial x} - \dfrac{\partial\tau_x}{\partial y}$	$-R\dfrac{\partial v}{\partial x} + R\dfrac{\partial u}{\partial y}$
N $\rightarrow$ S	≈ 0	< 0	< 0	≈ 0
S $\rightarrow$ N	≈ 0	> 0	< 0	$\gg 0$

Table 2: Sign of terms in the vorticity balance for northward and southward flow of a subtropical gyre. Columns 2 and 3 represent the change of relative and planetary vorticity (l.h.s. of 58) following the fluid; columns 4 and 5 give the signs of the production and dissipation terms of potential vorticity (r.h.s. of 58)

is to move northward stems from a strong dissipation of negative vorticity in the western boundary current through large negative values of $\partial v/\partial x$. Dissipation of negative vorticity then is sufficient to over-compensate the input of negative vorticity by wind stress. Hence, currents are intense only in the west. This argument was first presented by Stommel (1951).

We now turn to the deep circulation. In this case change of potential vorticity due to friction is neglected. A water column extending from the ocean bottom to some intermediate depth in the ocean is loosing mass continuously though its top because of the uniform upwelling Q (see Fig. 9), and hence $Q > 0$. Consider now the situation in the northern hemisphere $(f > 0, f \gg \zeta)$. Potential vorticity must increase when moving with the fluid in the northern hemisphere since the right side of eq. 58 is positive. A water parcel can satisfy this requirement in a fluid layer of constant depth H if it increases its planetary vorticity f which implies northward movement. This is consistent with the results of the Stommel model in the interior (eq. 45). The same reasoning can be done in the southern hemisphere and the result is that movement in the geostrohpic interior subject to upwelling must be poleward.

3 Abrupt Climate Changes and the Ocean

3.1 Multiple Equilibrium States of the Circulation

The idea that the ocean has more than just a regulating or damping effect on climate changes is old. The American geologist T. C. Chamberlin who has made significant contributions to the understanding of the ice ages already wrote in 1906 (Chamberlin 1906):

> "In an endeavor to find some measure of the rate of the abysmal circulation, it became clear that the agencies which influence the deep-sea movements in opposite phases were very nearly balanced. From this sprang the suggestion that, if their relative values were changed to the extent implied by geological evidence, there might be a reversal of the direction of the deep-sea circulation, and that this might throw light on some of the strange climatic phenomena of the past and give us a new means of forecast of climatic states in the future."

This statement already contains the important ingredients that are responsible for what we today call "multiple equilibria". The topic was then dormant for some 50 years until Stommel (1961) formulated a 2-box model that exhibited 2 stable equilibrium states. In his conclusions he wrote:

> "One wonders whether other, quite different states of flow are permissible in the ocean or some estuaries and if such a system might jump into one of these with a sufficient perturbation. If so, the system is inherently fraught with possibilities for speculation about climatic change."

These early insights were forgotten for another 20 years until marine sediment cores were analyzed in sufficiently high temporal resolution. One example is the study of Ruddiman and McIntyre (1981) that showed that the Younger Dryas cold event (11,000–10,000 BP ^{14}C-years) was associated with a rapid southward movement of the North Atlantic polar front by more than 20° latitude. This, combined with evidence of CO_2-changes in ice cores, lead Oeschger *et al.* (1984) to suggest that rapid changes of the ocean circulation are responsible for the variations found in the paleoclimatic archives. The "target" for modelers was formulated by Broecker *et al.* (1985), and the first 3-dimensional ocean model showing multiple equilibria followed soon (Bryan 1986). It was this study that finally convinced researchers that the ocean takes a central and *active* role in the climate system.

Bryan (1986) reasoned that the water sinking in the high latitudes is fed from the lower latitudes where the salinity is higher. This operates as a positive feedback mechanism for deep water formation. Assume that this surface mass flux is temporarily reduced: the salinity then decreases and deep water formation is reduced. This in turn reduces the advection of low-latitude high-salinity waters further and results in a rapid switch-off of the thermohaline circulation on time scales of decades. A "polar halocline catastrophe" ensues which is characterized by very low surface salinities in the former sinking regions (Bryan 1986; Weaver and Sarachik 1991b; Wright and Stocker 1991; Weaver *et al.* 1993; Zhang *et al.* 1993). As a result, the thermohaline circulation is interrupted or even reversed implying large changes in the meridional heat fluxes, in sea surface temperature and sea surface salinity. Such different states could also be realized in newly developed 2-dimensional thermohaline models (Marotzke *et al.* 1988; Wright and Stocker 1991; Stocker and Wright 1991b; Stocker and Wright 1991a), multi-basin 3-dimensional ocean models (Maier-Reimer and Mikolajewicz 1989; Marotzke and Willebrand 1991; Hughes and Weaver 1994) and coupled atmosphere-ocean models (Manabe and Stouffer 1988; Stocker *et al.* 1992).

Here, we will give a basic introduction of the dynamical mechanisms responsible for multiple equilibrium states. As was shown in the last section, most of the depth-integrated meridional heat flux in the ocean is due to the thermohaline circulation, i.e. the flow that consists of S_0, the DWBC, DGF and a return flow near the surface. In the zonal average of Fig. 9, displayed in Fig. 11 the thermohaline circulation appears as a continuous flow, often called "conveyor belt" (Broecker 1991; Schmitz 1995; Macdonald and Wunsch 1996). Although suggestive, this term should be used with caution. From the 3-dimensional model we have learned that the deep flow consists of two regimes: a strong DWBC and a gentle northward flow in the geostrophic interior (DGF). Since the DWBC is fed by both S_0 and the recirculating DGF, the zonal average is not zero, and a "lower limb" of the "conveyor" results. Properties of the water masses in the DWBC (T, S, tracers) can be followed over long distances, and therefore, this part may be loosely referred to as a "conveyor" circulation (Gordon 1986; Macdonald and Wunsch 1996). The "upper limb", on the other hand, is clearly not a "conveyor" circulation: the water is in continuous exchange with the atmospheric water cycle. Precipitation and evaporation change the properties of the surface waters relatively quickly.

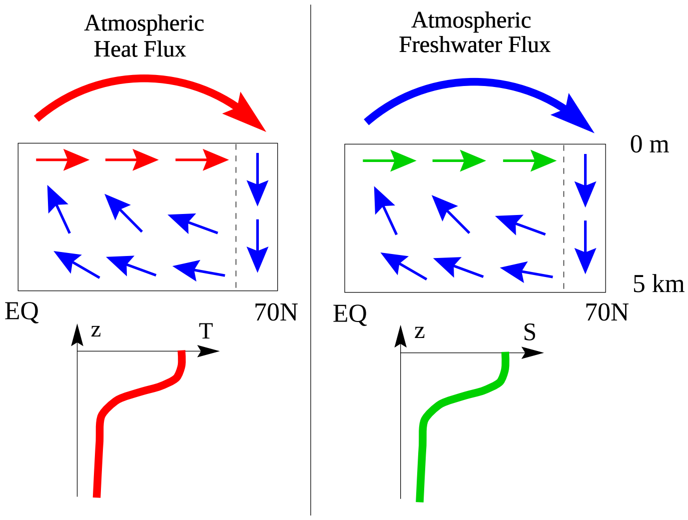

Figure 11: Conceptual representation of the zonal average of the complex flow in Fig. 9 which appears as a simple closed loop, "conveyor belt". The left column displays the cycle of heat. Due to the planetary energy balance heat must be transported polewards to which atmosphere and ocean contribute about equally. The right column shows the cycle of salt (or negative freshwater) in the ocean: freshwater is released due to net evaporation in the atmosphere of the low latitudes and taken up in the high latitudes, implying a northward meridional flux of freshwater in the atmosphere and a northward meridional flux of salt in the ocean. The circulation is direct with respect to T, i.e. cold waters are sinking in the north. Sinking waters are fresh but the effect of temperature on density is dominant. The transport of fresh water in the combined system atmosphere-ocean describes a closed loop. [From Wyrtki 1961, with additions]

The thermohaline circulation is driven by fluxes of buoyancy, i.e. density, through the ocean surface to which both heat and freshwater fluxes contribute. Take a situation typical for the North Atlantic. In low latitudes, the flux of heat is directed into the ocean and reduces density, while in high latitudes the ocean loses heat to the atmosphere and hence densities increase (Fig. 11). The hydrological cycle, on the other hand, provides the freshwater fluxes: evaporation exceeds precipitation in the subtropics. This increases density, whereas the opposite is the case closely around the equator and the mid to high latitudes. Therefore, temperature tends to drive the thermohaline circulation while the hydrological cycle acts as a brake.

It is important to note that the advection of saline waters from lower latitudes is essential for the deep water formation process. Were the salinity of the northward flowing waters lower than about 34.6 psu, cooling to even the freezing point would not increase the density sufficiently (to about 1027.8 kg/m^3) to permit deep water formation. Assume now that there is still evaporation in the low latitudes (higher air temperatures) and precipitation in the high latitudes: the freshwater flows northward in the atmosphere. If – for reasons explained below – cooling in the atmosphere is not sufficient to initiate deep water formation, the circulation must reverse (Fig. 12). Furthermore, to close the global hydrological cycle, the surface water flowing southward must now be fresher than the deep waters flowing north, i.e. the stratification with respect to salinity has reversed. Stratification with respect to temperature does not reverse but weakens considerably, and hence the oceanic meridional heat transport is diminished in magnitude and southward. This leads to a high-latitude

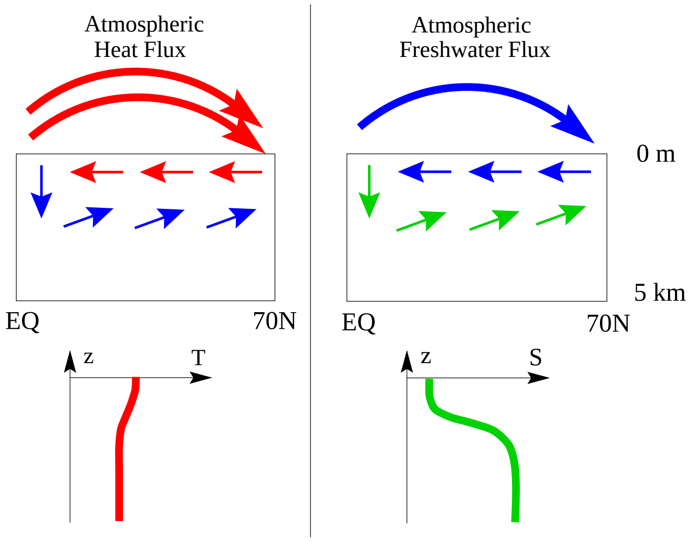

Figure 12: As Fig. 11 but for a reversed and shallowed circulation. The left column displays the cycle of heat in the ocean: the meridional heat flux in the ocean is reversed and significantly reduced in magnitude due to an almost vertically uniform temperature profile. In consequence, the planetary energy balance requires a stronger meridional heat flux in the atmosphere in order to compensate changes in oceanic heat flux. The right column shows the cycle of salt (or negative freshwater) in the ocean which is unchanged: freshwater is released in the low latitudes and taken up in the high latitudes, implying a northward meridional flux of freshwater in the atmosphere and a northward meridional flux of salt in the ocean. For the same direction of the water cycle (compare Fig. 11), the ocean circulation can reverse only if the vertical salinity distribution is changed.

cooling and a strongly enhanced meridional heat flux in the atmosphere that must partly compensate the reduction in oceanic heat flux in order to satisfy the planetary energy balance. It turns out that the second state (Fig. 12) has lower potential energy in this conceptual model than the state in Fig. 11 and an increased stability is expected.

The existence of multiple equilibria in the ocean can be demonstrated quantitatively in the complete hierarchy of ocean models and is thus a robust result of the models (see review by Weaver and Hughes (1992)). The basic idea is explained here following Marotzke (1990) who formulated a simplified version of the box model by Stommel (1961). The model consists of only two boxes: a box representing the low-latitudes with warm temperatures and one for the high latitudes where the temperatures are cold (Fig. 13). The temperature difference, ΔT, between the boxes is held fixed. The salt balance is given by

$$\dot{S}_1 = |q| \cdot (S_2 - S_1) + P \ , \quad \dot{S}_2 = |q| \cdot (S_1 - S_2) - P \quad , \tag{60}$$

where q is a meridional water transport and S_1 and S_2 are the salinities in the low and high-latitude boxes, respectively (Fig. 13). The transport is assumed to be proportional to the density difference between the boxes:

$$q = k \cdot (\rho_2 - \rho_1) = k\alpha \cdot (T_2 - T_1) + k\beta \cdot (S_2 - S_1) \quad , \tag{61}$$

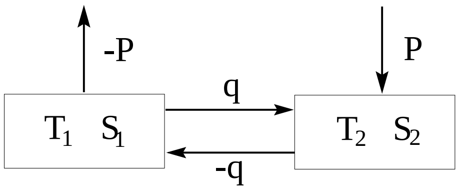

Figure 13: A 2-box version of the world ocean. Water is exchanged between a low (T_1, S_1) and a high-latitude box (T_2, S_2) at rate q. The cycle of freshwater is closed through an "atmosphere" in which precipitation P is negative in the low and positive in the high latitudes, i.e. northward water transport. [From Marotzke 1990]

based on (6) neglecting the non-linear term. Steady states of (60) are given by

$$\Delta S = \begin{cases} -\dfrac{\alpha \Delta T}{2\beta} \pm \sqrt{\left(\dfrac{\alpha \Delta T}{2\beta}\right)^2 - \dfrac{P}{k\beta}} \ , \quad q > 0 \\ \\ -\dfrac{\alpha \Delta T}{2\beta} + \sqrt{\left(\dfrac{\alpha \Delta T}{2\beta}\right)^2 + \dfrac{P}{k\beta}} \ , \quad q < 0 \end{cases} \tag{62}$$

Substituting the positive non-dimensional quantities

$$\delta = -\frac{\beta \Delta S}{\alpha \Delta T} \ , \quad E = \frac{\beta P}{k(\alpha \Delta T)^2} \quad , \tag{63}$$

into 62 we obtain

$$\delta = \begin{cases} \frac{1}{2} \pm \sqrt{\frac{1}{4} - E} \ , \quad q > 0 \\ \\ \frac{1}{2} + \sqrt{\frac{1}{4} + E} \ , \quad q < 0 \end{cases} \tag{64}$$

We note that for a direct circulation (cold waters are sinking) $q > 0$. Equation 64 implies that for $E < 0.25$ there are two equilibrium states with a direct circulation, and one equilibrium state with an indirect circulation. It can be shown that the state with the intermediate δ is not stable. When E increases, i.e. precipitation in the high-latitude box becomes stronger, the number of equilibrium states is reduced to one for $E > 0.25$. For large P or small ΔT, i.e. $E > 0.25$, only the indirect circulation is a steady state, in other words the circulation has changed direction. The effect of salinity on density is now dominant and waters are sinking in the low-latitude box (see also Fig. 12).

The reason for multiple equilibria lies in the physics of the different components of the surface buoyancy flux. Sea surface temperature (SST) anomalies create local heat flux anomalies that tend to erase the SST anomalies effectively since fluxes are essentially proportional to the temperature difference between the ocean and the atmosphere. Sea surface salinity (SSS) anomalies, on the other hand, have no influence on freshwater fluxes nor on heat fluxes implying that SSS anomalies will have a much longer residence time on the ocean surface. To account for this fact in models, one uses "mixed boundary conditions", i.e. heat fluxes are proportional to temperature differences between ocean and atmosphere whereas freshwater fluxes are held constant (Rooth 1982). For this reason, SSS anomalies are crucial for a number of dynamical effects of the thermohaline circulation. Based on these considerations Welander (1986) has presented a "gallery" of thermohaline oscillators.

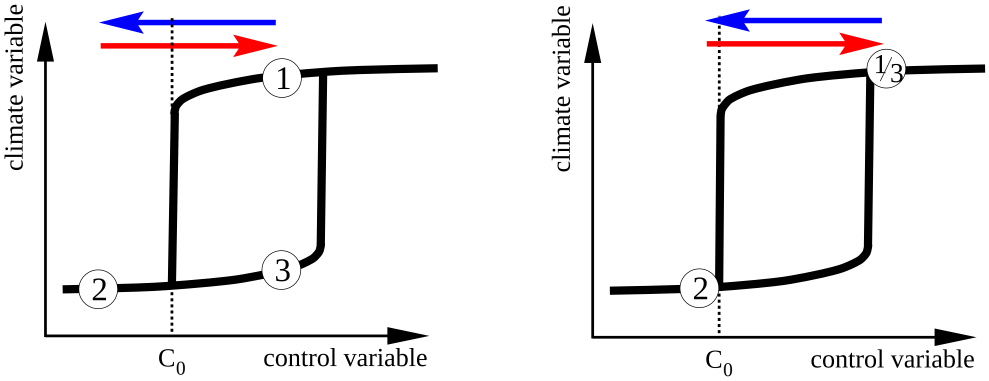

Figure 14: Ocean models exhibit a hysteresis behaviour as a function of a control variable (e.g. surface freshwater balance in the North Atlantic). For a range of values multiple equilibria are possible, i.e. the climate variable (e.g. sea surface temperature, SST, in the North Atlantic) can take more than one value. A given perturbation causes an abrupt change in the climate variable (1→2) and stays in the new equilibrium (3), depending on the exact location of the present state (1) with respect to the hysteresis (left panel). The same change of the control variable can induce only a temporary transition (right), if the initial state is a unique equilibrium. A transition does occur only if a critical threshold value C_0 of the control variable is passed. [From Stocker and Wright 1991a, with additions]

Because the thermohaline circulation accounts for most of the meridional heat flux in the ocean, possible changes in this circulation affect the sea surface temperature significantly and can alter the regional climate considerably. Due to instabilities, changes can be fast which is another characteristic feature of high-resolution paleoclimatic records (Dansgaard *et al.* 1989; Lehman and Keigwin 1992; Taylor *et al.* 1993). We now turn to an example of the last of such fast changes of climate and present some examples how models can provide insight into the dynamics of the climate system.

3.2 Younger Dryas: The Last Great Cold Event

a) Deep Circulation

Changing precipitation in the high latitudes is not the only mechanism that affects deep water formation. In general, the surface freshwater balance in the North Atlantic is a control variable of the system since it determines to a large extent the density of surface waters. Changes between states can therefore be induced also by glacial meltwater from disintegrating ice sheets. Glacial meltwater was not continuously delivered to the ocean during the last deglaciation where about $40 \cdot 10^6\,\mathrm{km}^3$ of ice was melted which rose sea level by about 120 m. Corals, which live in the top 5 m of the ocean, are good recorders of sea level. Their dating shows that two distinct pulses of meltwater occurred (Fairbanks 1989; Edwards *et al.* 1993). The maximum strength was estimated at about 0.5 Sv which is much larger than the perturbations needed to induce rapid circulation changes in ocean models (Maier-Reimer and Mikolajewicz 1989; Stocker *et al.* 1992; Rahmstorf 1994). The exact timing of these pulses is under discussion, but it is clear that the Younger Dryas (YD) cold event (about 12,800–11,650 BP) started after the first pulse (Bard *et al.* 1996).

The possible responses of the climate system depend on the structure and exact location

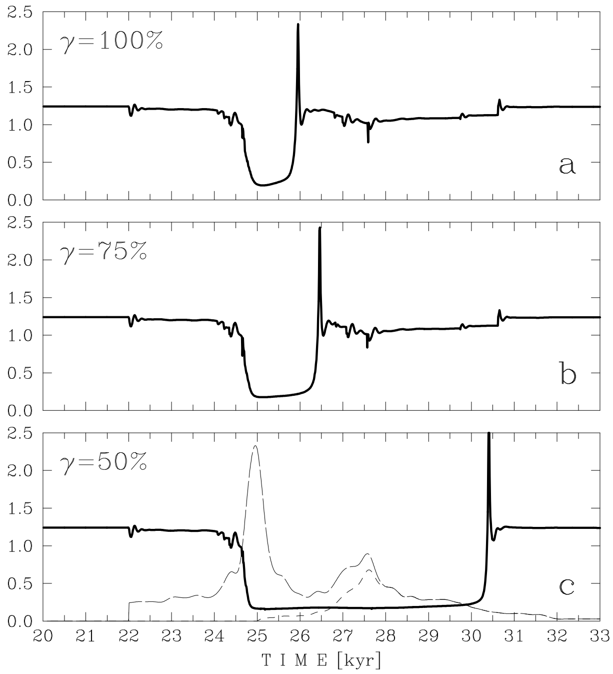

Figure 15: Evolution of the Atlantic meridional heat flux across 32.5°N in PW (1 PW=10^{15}W). The three panels correspond to cases in which the runoff into the North Atlantic at high latitudes is reduced by (a) 100%, (b) 75%, and (c) 50% relative to present-day values as the meridional heat flux is reduced to zero. The meltwater discharge into the North Atlantic and Southern Ocean are indicated by the long and short dashed lines in (c), respectively, on a scale of 0–0.5 Sv. [From Stocker and Wright 1996].

of the various steady states in parameter space. This was first shown by Stocker and Wright (1991a) (Fig. 14). For a given temporary reduction of the control variable (surface freshwater balance in our case), indicated by the horizontal arrows the system makes a transition to a different equilibrium state, if a threshold value is crossed. The transition can be permanent (Fig. 14, left) or temporary (Fig. 14, right) depending on the location of the initial state on the hysteresis curve. Ocean models can exhibit quite complicated hystereses as was shown by Mikolajewicz and Maier-Reimer (1994) and Rahmstorf (1995). The solution structure depends on the exact parameterisation of the surface fluxes, and on the given forcing fields.

A shut-down of an active thermohaline circulation due to the addition of freshwater is simulated by all ocean models that incorporate mixed boundary conditions or more advanced parameterisations of surface fluxes. Most models, however, tend to be *hypersensitive* and exhibit *permanent circulation changes* induced by small perturbations (Maier-Reimer and Mikolajewicz 1989; Marotzke and Willebrand 1991; Stocker *et al.* 1992).

To find a remedy, we have studied the sensitivity of the circulation as a function of the strength of the hydrological cycle in the atmosphere (Wright and Stocker 1993). Using a zonally averaged, dynamical, coupled atmosphere-ocean climate model (Stocker *et al.* 1992) we show that the solution structure can be changed in such a way that the mode change is reversible, i.e. once the perturbation of the surface freshwater balance decreases below a minimum threshold, the conveyor belt circulation switches on again. There is direct

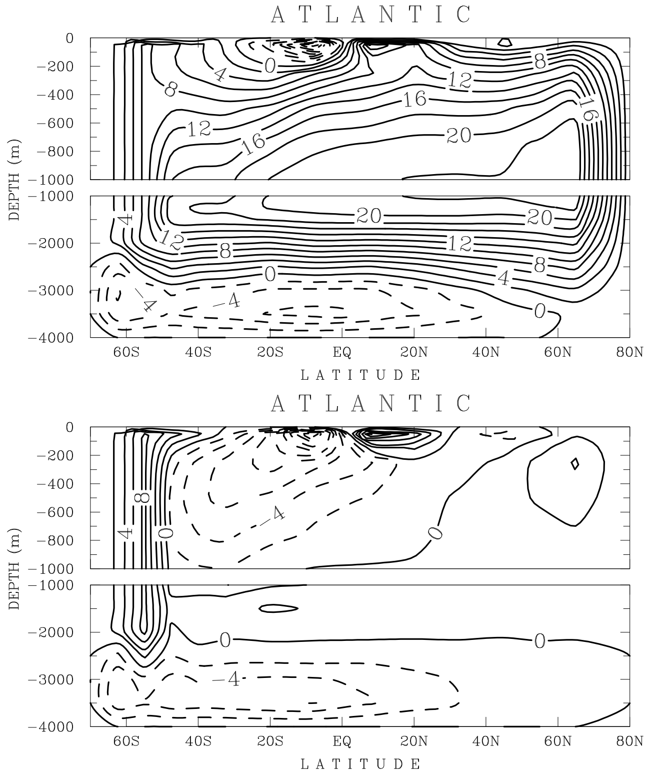

Figure 16: Atlantic transport streamfunction before (top) and during (bottom) the cold event for the experiment of Fig. 15b, where deep water formation is shut off for about 1200 years. [From Stocker and Wright 1996].

indication from the paleoclimate record that the hydrological cycle has changed significantly from the glacial to the present Holocene (Alley *et al.* 1993), justifying this approach.

Figure 15 shows the different possible transient responses to a meltwater event. The model includes a runoff feedback, i.e. if there is a cooling in the Atlantic region, continental runoff is reduced by a factor γ relative to the modern runoff which is estimated from Baumgartner and Reichel (1975). The first meltwater pulse causes a collapse of the thermohaline circulation in the Atlantic which initiates the cold event. The duration of the cold event can be controlled by the specification of the feedback strength.

The reduction of the meridional heat transport is due to drastic changes in the circulation of the North Atlantic (Fig. 16). The transition occurs within a few decades. Before the cold event deep water formation is active in the Atlantic, while during it there is almost no northward flow in the upper layers except for the Ekman transport.

During the event, the deep Atlantic is decoupled from the surface. The shut-down of the meridional heat flux causes a strong cooling of the upper 1000 m. This is shown in Fig. 17. The model predicts an antisymmetric climate change in the Atlantic with respect to latitude. While the northern part cools down, there is warming in the intermediate part of the Southern Ocean. Temperature changes in the Pacific are moderate but there is a near-surface cooling observed in the northern part. This is due to a general decrease of atmospheric surface temperatures in this latitude band caused by a dramatic decrease of

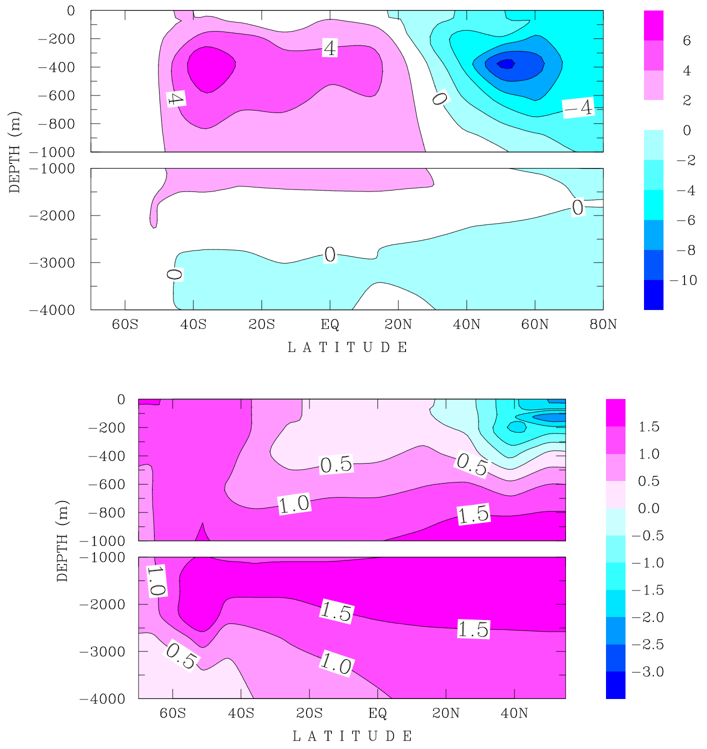

Figure 17: Temperature difference between the cold state (Fig. 16, bottom) and the unperturbed state (Fig. 16, top) of the thermohaline circualtion. Changes in the Atlantic are large and of opposite signs in both hemispheres, while the Pacific experiences comparatively little changes.

SST in the Atlantic.

Interhemispheric antisymmetry is an unexpected, but physically entirely plausible feature of the climate system and has received increased attention (Broecker 1997; Broecker 1998). It is telling evidence for the fundamental role of the ocean during abrupt change. The basis of the mechanism lies in the fact that an active thermohaline circulation in the Atlantic ocean is associated with a depth-integrated meridional heat flux that is directed northward at all latitudes (see Fig. 2). This implies that the Atlantic draws heat from the Southern Ocean and actually cools it (Crowley 1992). If the circulation breaks down and the north cools in consequence, e.g. during Younger Dryas, the excess heat accumulates in the Southern Ocean hemisphere which leads to a warming. This is actually observed in the paleoclimatic record (see below), especially in the high-resolution polar ice cores from Greenland and Antarctica (Blunier *et al.* 1997; Blunier *et al.* 1998). The prerequisite for paleoclimatic records to address this question is excellent time resolution and a common time scale (either absolute or synchronised) better than, say, 200 years for records from different locations; wiggle matching[‡] should be avoided. A sufficiently precise time scale is difficult to obtain

[‡]Wiggle matching assumes that climatic events in different paleoclimatic archives happen at the same time. This is a common method in paleoclimatology and bypasses the question of leads and lags because of the implicit assumption of synchroneity of events. As a technique, it is only permissible for records whose distance in geographical location is smaller than the typical length scale of the physical process responsible for the changes that are analysed.

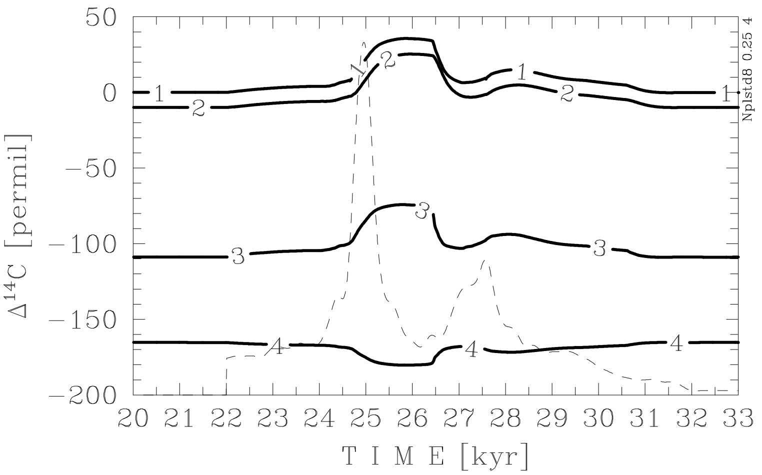

Figure 18: Evolution of mean Δ^{14}C in the major reservoirs for the experiment in Fig. 15b. The radiocarbon inventory increases in atmosphere (1), biosphere (2) and the upper 1000 m of the ocean (3) while it decreases in the deep ocean (4) due to reduced ventilation. [From Stocker and Wright 1996].

as radiocarbon has special problems during times when ocean ventilation changes dramatically (Stocker and Wright 1996; Hughen *et al.* 1998); this issue will be addressed in the following section. Uncertainties in the time scale preclude conclusions regarding the global synchroneity of Younger Dryas or other abrupt events (Denton and Hendy 1994). As we have shown, there are global effects but they are not necessarily of the same sign.

b) Radiocarbon

Such rapid changes also have important implications for other components of the climate system such as the global carbon cycle or the cryosphere (ice sheets). Part of the carbon cycle is the carbon isotope ^{14}C, a radionuclide with a half life of 5730 years. It is produced in the stratosphere by cosmic radiation and enters the carbon cycle in the form of $^{14}CO_2$. While being an excellent dating tool for many purposes, the atmospheric concentration of radiocarbon also tells us something about the global ventilation rate of the ocean. Since the ocean carbon reservoir is about 60 times larger than the atmosphere and about 20 times larger than the terrestrial biosphere, most of the ^{14}C produced in the stratosphere ends up in the ocean. Assuming a constant production rate in the stratosphere, any changes to the exchange fluxes leaving the atmosphere will have an impact on the atmospheric concentration of ^{14}C.

Figure 18 shows the evolution of the concentration of radiocarbon in the major reservoirs of the climate system. A reduction of the deep water formation during the cold event leads to an increase of ^{14}C in all reservoirs that are exchanging directly with the atmosphere while a decrease is found in the deep ocean.

Changes of the atmospheric concentration of radiocarbon influence the ability of dating samples using this method. This is illustrated in Figure 19. If the atmospheric concentration remains constant, a sample's age can be simply determined by calculating the time elapsed from the initial atmospheric concentration to the measured current concentration. The

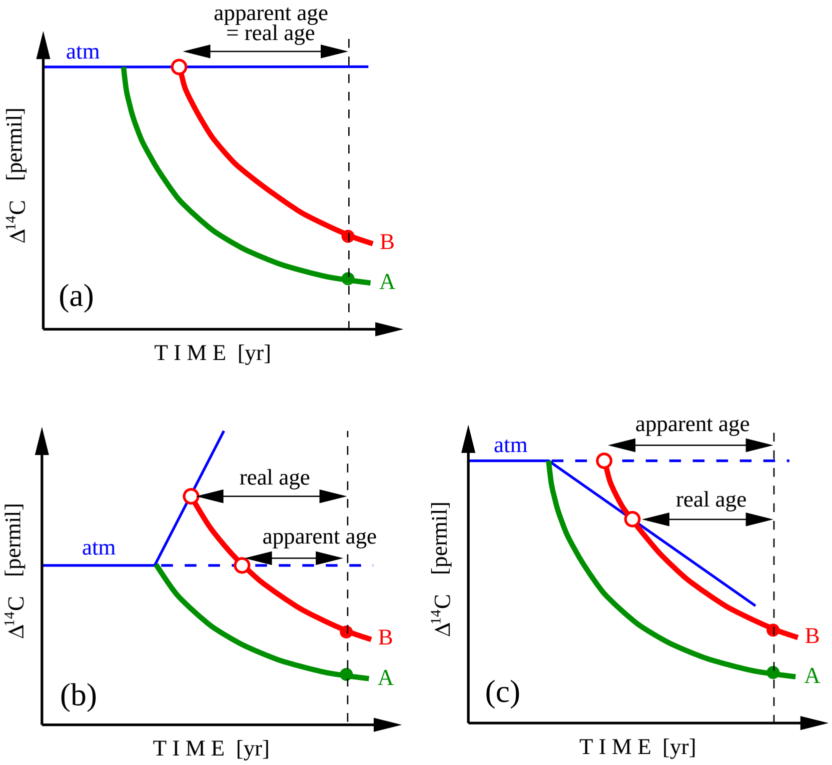

Figure 19: Schematics of different cases of a variable atmospheric radiocarbon concentration. If the atmospheric concentration remains constant, samples A and B can be easily dated by calculating the time elapsed during the decay of the concentration to the current value (a). If the atmospheric concentration increases, (b), the real age is larger than the apparent age (the clock speed up), which assumes a constant atmospheric concentration. If, on the other hand, the atmospheric concentration decreases, (c), the real age is smaller than the apparent age and the clock slows down.

latter is lower due to the decay of ^{14}C (Fig. 19a). However, if the atmospheric concentration has changed in the meantime, one has to distinguish between an 'apparent age' and the 'real age'. If the atmospheric concentration increases (Fig. 19b), the real age is larger than the apparent age, which is based on the assumption of constant atmospheric concentration. One can interpret this as a speed-up of the radiocarbon clock (Fig. 19b). On the other hand, in the case of a decreasing atmospheric concentration the real age is smaller than the apparent age. One can interpret this as a slow-down of the radiocarbon clock (Fig. 19c). In the extreme case where the atmospheric concentration decreases at the same rate as the natural decay, radiocarbon dating becomes impossible and the radiocarbon clock comes to a halt. This manifests itself, for instance, as nearly equal radiocarbon ages over entire sections of sediment cores and is referred to as a “radiocarbon plateau”. Such plateaus have been measured in lake sediments (Oeschger *et al.* 1980; Zbinden *et al.* 1989), in absolutely dated tree rings (Kromer and Becker 1993), and in varved lake sediments (Goslar *et al.* 1995; Björck *et al.* 1996). An example of the dated tree ring series is given in Fig. 20 where the long plateau at the end of Younger Dryas (YD) is indicated by the grey box.

The model experiment above gives a plateau at the end of the cold event. However, its duration is only about 50 years, much shorter than the plateaus found in the paleoclimatic archives. Possibile mechanisms for longer duration are the concurrent increase of CO_2 in the

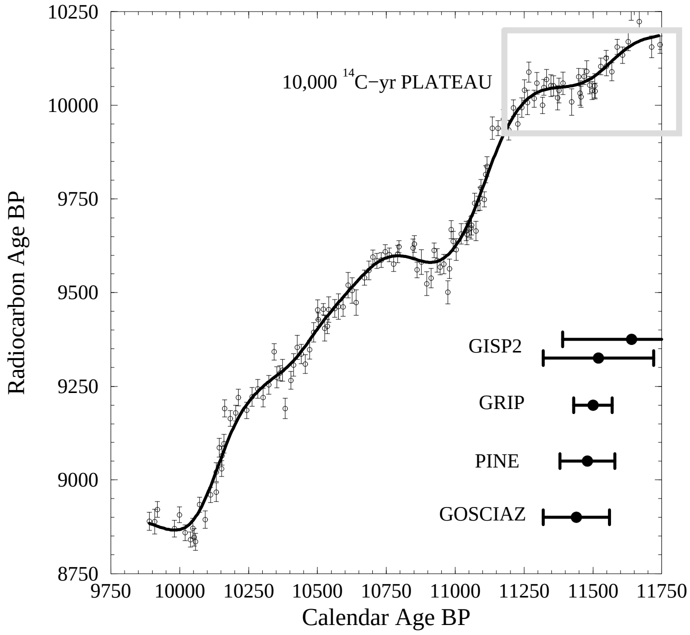

Figure 20: Oldest part of the radiocarbon calibration curve derived from the combined oak/pine German master chronology by Kromer and Becker (1993) and recently corrected by *Kromer* [pers. comm.] showing a short age plateau at 9,600 ^{14}C-yr and the extended period of strongly reduced radiocarbon age increase referred to as the 10,000 ^{14}C-yr plateau (grey box). The beginning of the pine chronology (8,800 ^{14}C-yr) is tied to the oak chronology through the long-term ^{14}C-trend. Recent estimates of the termination of the Younger Dryas event (YD) are indicated by the horizontal bars. The 10,000 ^{14}C-yr plateau ends about 300 years after the termination of the YD based on the pine tree ring width (Björck *et al.* 1996) or 300–450 years after the termination according to the dating of the two Greenland ice cores (Johnsen *et al.* 1992; Alley *et al.* 1993). Data from Polish lake Gościąż show that the 10,000 ^{14}C-yr plateau ends 250 years after the termination of YD (Goslar *et al.* 1995). All estimates are in close agreement and indicate that the 10,000 ^{14}C-yr plateau extended a few hundred years beyond the cold-warm transition at the end of YD (calibration curve supplied by *Kromer* [pers. comm.]).

atmosphere at the YD termination or a much larger sea ice extent during YD. A sensitivity study indicates that the plateau length can increase to about 250 years (Stocker and Wright 1996).

c) Atmospheric Carbondioxide

Thanks to the excellent paleoclimatic archive of polar ice cores, we have direct observations of the evolution of CO_2 during YD Fig. 21. Atmospheric CO_2 serves as a global parameter to test our hypothesis that the thermohaline circulation exhibited dramatic changes with the associated antisymmetric coupling of the hemispheres. Had YD been a global cooling, we would expect a decrease of sea surface temperature by about 2–3°C globally. The solubility of CO_2 at the ocean's surface is temperature dependent: a reduction of 1°C SST leads to

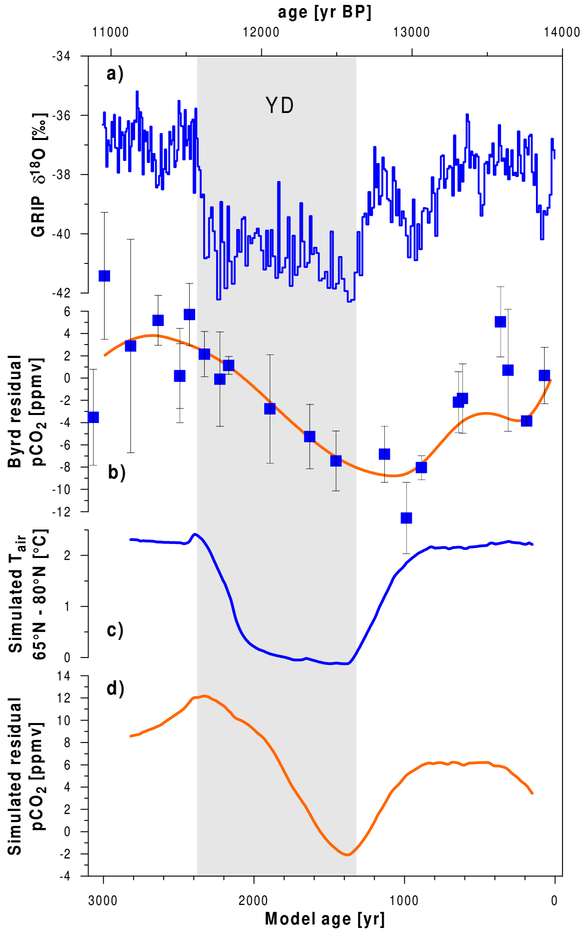

Figure 21: Physical and biogeochemical changes during the last abrupt climate event of the Younger Dryas (YD, 12.7–11.6 kyr BP, shaded). (a) GRIP δ^{18}O record indicating abrupt cooling and warming at the beginning and the end of YD, respectively. (b) Residual $p\mathrm{CO}_2$ from the Byrd ice core calculated by subtracting the long-term linear increase from 18 kyr BP to 10 kyr BP from the measurements (Blunier *et al.* 1997). (c) Air temperature changes simulated by the 2.5-D model of Stocker and Wright (1996) due to a meltwater event. (d) Changes of atmospheric CO_2 using the physical-biogeochemical model of Marchal *et al.* (1998b).

a decrease of atmospheric CO_2 of about 10 ppm (Takahashi *et al.* 1993). Thus, YD would manifest itself as a drop of atmospheric CO_2 by about 20–30 ppm; this could be clearly distinguished in a polar ice core. First measurements do not show this decrease, instead an almost linear increase of CO_2 is observed (Blunier *et al.* 1997). First experiments with a low-order physical-biogeochemical model exhibit such an increase of CO_2 during an abrupt cooling event induced by glacial melting (Marchal *et al.* 1998a). This suggests that the cooling at the sea surface that occurred during YD in the northern North Atlantic and the northern hemisphere (Lehman and Keigwin 1992; Kennet and Ingram 1995) must have been compensated by a warming elsewhere. This, however, is consistent with the postulated antisymmetric coupling of the hemispheres during abrupt climate events. Therefore, CO_2

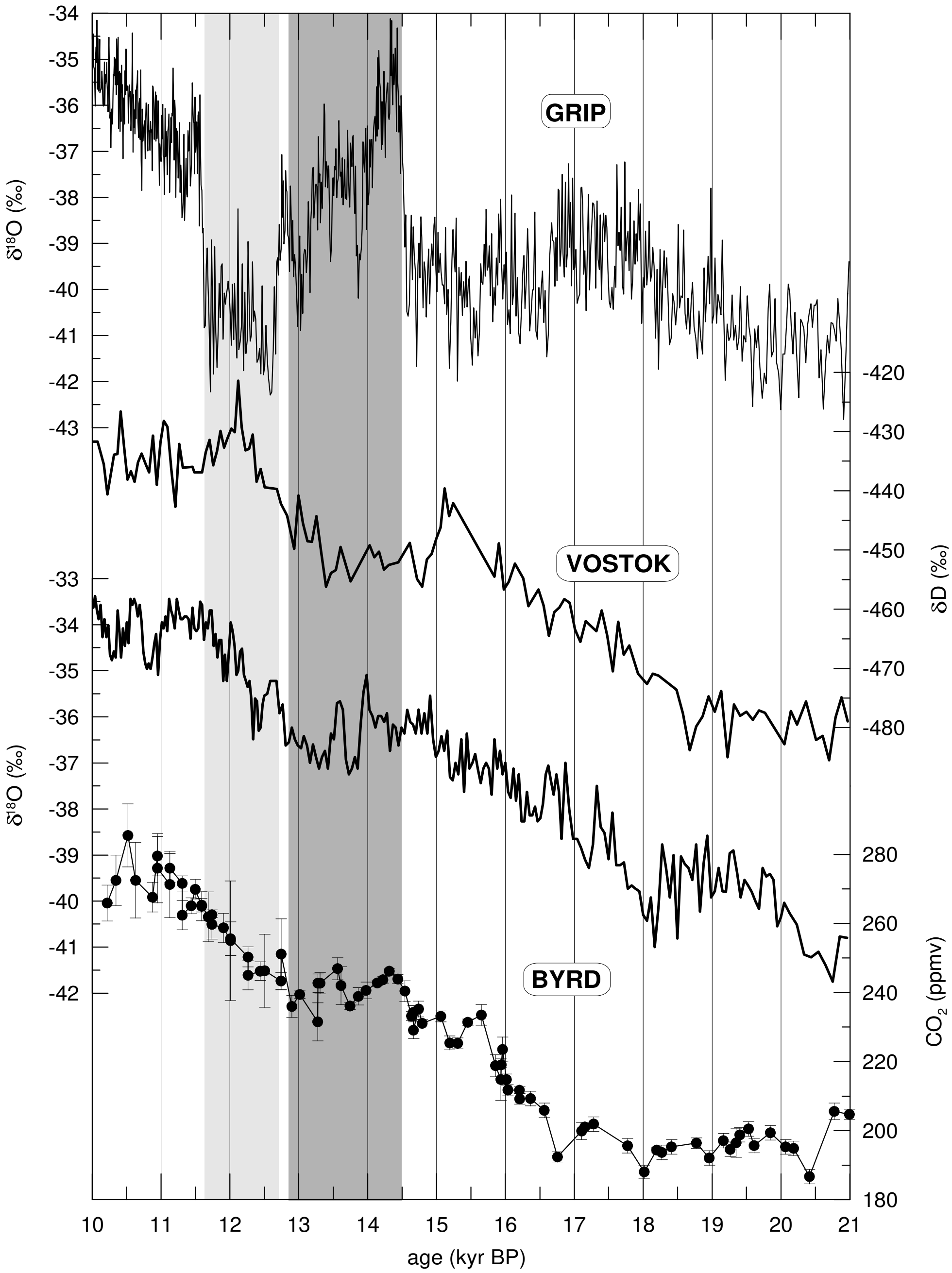

Figure 22: High-resolution climate records based on polar ice cores from Greenland and Antarctica during a sequence of abrupt climate changes in the northern hemisphere. Changes in the isotopic composition of the water molecule, δ^{18}O and δD, indicate temperature variations. Atmospheric CO_2 is measured in bubbles enclosed in Antarctic ice from Byrd station (Blunier *et al.* 1997) and increases almost linearly during YD. At 16,500 yr BP the warming during deglaciation is well under way in Antarctica while it is suppressed in Greenland probably due to Heinrich event 1. The transition into the Bølling warm phase is abrupt and probably initiates the cooling in Antarctica (Antarctic Cold Reversal). This slight cold phase is interrupted at the time YD begins in the northern hemisphere at 12,700 yr BP. The northern cold phase is coeval with the resumption of warming in the south which is, again, interrupted when YD terminates. This sequence strongly suggests an antiphase coupling of northern and southern hemispheres during sequences of abrupt climate change. [Figure from Blunier *et al.* 1997]

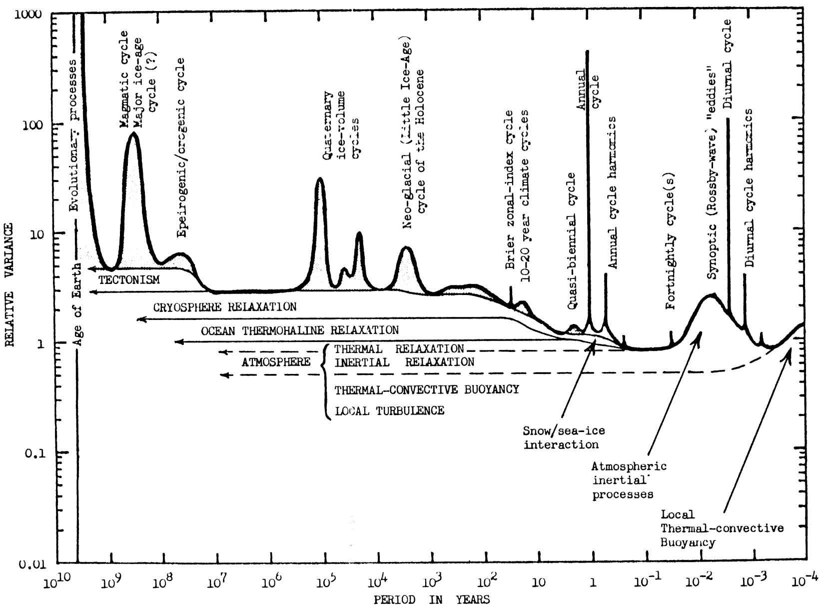

Figure 23: The original Figure of Mitchell (1976) showing a schematic spectrum of climate variability which is a composite of a red noise background due to stochastic fluctuations and distinct peaks resulting from various external forcings. Note that no peaks are in the El Niño and decadal-to-century band [From Mitchell 1976].

provides circumstantial and additional evidence for this important mechanism.

d) Summary and Outlook

While our model accounts for several important features of YD, recent paleoclimatic reconstructions of atmospheric methane concentrations (Chappellaz *et al.* 1993), mountain glaciers (Thompson *et al.* 1995) and Antarctic ice cores (Mayewski *et al.* 1996) indicate a global nature of the event where the low latitudes, in particular the hydrological cycle, play an important role. However, it has become clear from the above results, that many of these studies do not satisfy the stringent requirements regarding time control. The polar ice cores from Greenland and Antarctica are synchronised on the basis of variations in the atmospheric methane concentration with an uncertainty of less than 200 years (Blunier *et al.* 1997). We find that, superimposed on the world-wide warming during deglaciation, abrupt climate transitions at 14,500, 12,700 and 11,650 yr BP found in the north correlate with smoother changes *of the opposite sign* in the south (Fig. 22).

Other prominent examples of abrupt change are found in the marine and ice core records throughout the last glacial. Rapid events, Dansgaard/Oeschger cycles, are linked to the periodic discharge of icebergs from the northern hemisphere ice sheets into the Atlantic (Heinrich events) on the basis of the analysis of the composition of debris found in marine sediment cores (Broecker 1994). These massive discharges cause, after some delay, a pronounced warming in the North Atlantic region. First attempts with a box model indicate the feedback mechanisms between ocean, atmosphere and ice sheet that are necessary to produce this climate signal (Paillard and Labeyrie 1994; Stocker and Wright 1998).

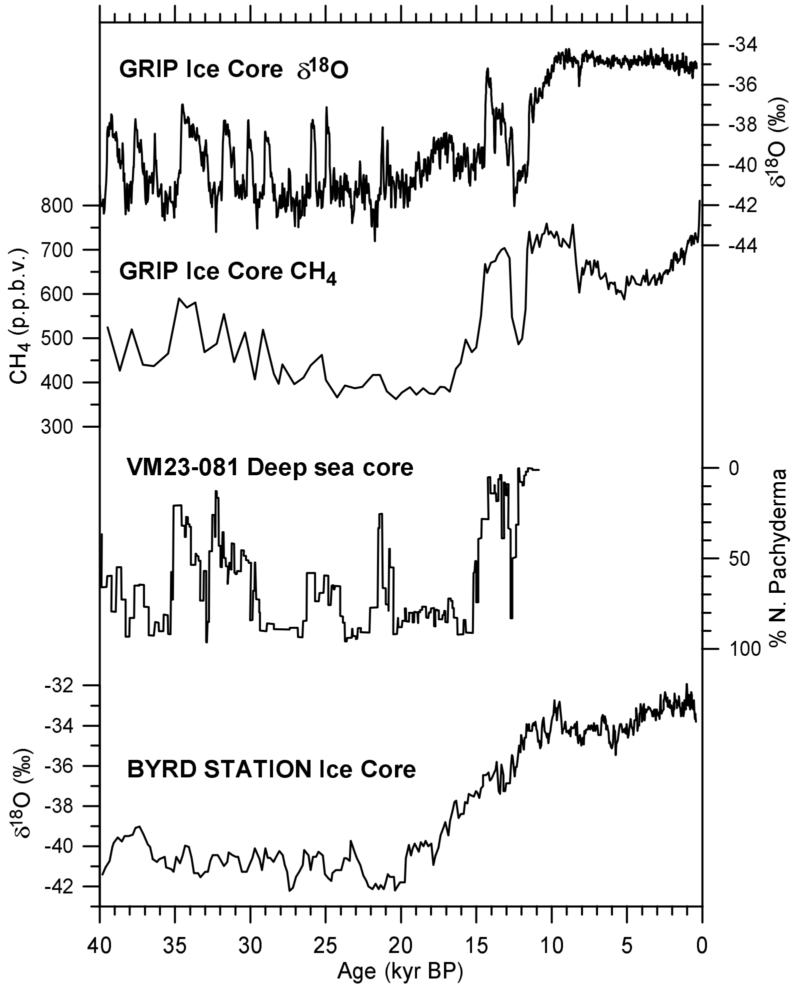

Figure 24: Climatic change over the last 40'000 years as obtained from the measurement of δ^{18}O on ice (from Johnsen *et al.* (1992), Dansgaard *et al.* (1993) and Hammer *et al.* (1994)) and CH_4 on air of bubbles trapped in the ice core (from Chappellaz *et al.* (1993) and Blunier *et al.* (1995). Four different features of climate variability are evident in the different time series: (i) slow, astronomically forced transition from the glacial to the interglacial (δ^{18}O records and CH_4); (ii) self-sustained oscillations during the glacial (foraminifera assemblages in a sea sediment core (from Bond *et al.* (1993)) and ice cores before 20 kyr BP); (iii) non-deterministic (chaotic) variability during the Holocene (δ^{18}O records); and (iv) abrupt reorganisations before 25 kyr BP and during the Bølling/Allerød/Younger Dryas Period (all but Byrd Station core) [Figure compiled by T. Blunier]

4 Natural Variability

This section closely follows a more complete review article (Stocker 1996).

4.1 Introduction

Variability is a fundamental property of our climate system. Mitchell (1976) proposed that the spectrum of climate variations is due to two different types of processes: internal stochastic mechanisms and external forcing mechanisms including their resonant amplification of internal modes. However, important aspects of climate variability are missing in this classical picture: e.g. self-sustained oscillations or natural variability generated *within* the climate system. Detection of anthropogenic climate change depends on our knowledge of the time scales and patterns associated with the natural level of variability on the decadal to century time scale.

Many aspects of Mitchell's schematic picture can be found in records of climatic data both, directly observed and proxy. For instance, the red noise background of the spectrum (i.e. longer time scales exhibit stronger spectral power) can be seen in observed data from the atmosphere and ocean, and model simulations exhibit very similar spectral characteristics (Delworth *et al.* (1993), their Fig. 2, reproduced here as Fig. 26). The spectra of longer time series (oxygen isotopes on planktonic foraminifera shells found in sea sediments) also confirm the red-noise continuum background and the presence of preferred time scales of variability (see e.g. Imbrie *et al.* (1992) and Imbrie *et al.* (1993)). Of more interest due to their predictive potential are the external mechanisms that produce variability on distinct time scales such as the diurnal and seasonal cycles, cyclic processes without a single distinct time scale such as ENSO, the Milankovic cycles and even slower, tectonic processes.

While this concept is a useful starting point, recent high-resolution paleoclimatic archives (see Fig. 24) have clearly demonstrated that additional aspects of climate variability must be taken into account. Four features of climatic change are evident in Fig. 24:

1. externally forced changes,
2. self-sustained oscillations,
3. non-deterministic variability,
4. abrupt reorganisations.

Various proxy and direct climatic data from the ice, sea and lake sediment archive illustrate the climatic evolution during the last 40,000 years. The transition from the last glacial to the Holocene is an **externally forced change** due to changes in the distribution of solar radiation and the operation of a number of feedback mechanisms due to greenhouse gases (foremost water vapor) and albedo (Imbrie *et al.* 1992; Imbrie *et al.* 1993). This is strong support for the Milankovic theory of climate change.

Climatic swings between milder and colder phases (Dansgaard/Oeschger cycles) during the glacial are most likely **self-sustained oscillations** of the Earth system (Bond *et al.* 1992; Bond *et al.* 1993; Paillard and Labeyrie 1994). **Non-deterministic variability** is visible indirectly in the δ^{18}O record of the last 10,000 years (Holocene) which fluctuates about a well defined mean value. This is a common feature of the climate system (Hasselmann 1976) and some modeling studies support this also for fluctuations on the decadal-to-century time scale (Saltzman 1983; James and James 1992; Roebber 1995). However, there are first indications that decadal-to-century time scale may actually be associated with well-organized and coherent changes in large-scale circulation patterns (Delworth *et al.* 1993; Mysak *et al.* 1993; Pierce *et al.* 1995).

Abrupt reorganisations are also recorded in sea sediments and ice cores: the abrupt warming into the Bølling/Allerød, the cooling initiating the Younger Dryas and its termination all occur on time scales of a few decades to a few years (Dansgaard *et al.* 1989; Taylor *et al.* 1993) and can be understood as shifts between different *equilibrium* states when system parameters are slowly changing (Stocker and Wright 1991a; Mikolajewicz and Maier-Reimer 1994; Rahmstorf 1995).

Solar forcing of periodic climate change on the decadal-to-century time scale has been a topic of debate for a long time. The sensitivity of the climate system to changes in the shortwave irradiation, however, seems to be rather small ($0.14\,\mathrm{K}/(\mathrm{Wm}^{-2})$, based on an AGCM simulation by Lean and Rind (1994)). Statistical analyses by Crowley and Kim (1996), on the other hand, indicate that at least a portion of the proxy time series can be correlated to solar cycles and that the variabiliy surface air temperature of the last few decades is to some, though minor, extent due changes in solar radiation (Hegerl *et al.* 1997).

4.2 Observational Evidence – Measurements and Proxy Records

Direct observations begin to exhibit large-scale climatic changes on the interdecadal time scale based on oceanic, atmospheric and geochemical data bases from the last 40 years (Roemmich and Wunsch 1984; Levitus 1989c; Parilla *et al.* 1994; Schlosser *et al.* 1991; Deser and Blackmon 1993; Kushnir 1994; Lazier 1996). Kushnir (1994) found that the difference between warm (1925–39, and 50–64) and cold years (1900–14, and 70–84) consists of positive SST anomalies in the region of south-east Greenland, the Canadian maritimes and the US east coast with associated sea level pressure patterns very similar to those reported by Deser and Blackmon (1993). Hydrographic changes in the shallow and intermediate North Atlantic reported by Levitus (1989a) and Levitus (1989b) are consistent with these findings. Schlesinger and Ramankutty (1994) analyze global data sets of surface air temperature covering the period 1858–1992 in 11 different geographical regions. They found a 50–80 year cycle in various sub-regions of the globe with the largest amplitudes in the North Atlantic and North American regions indicating the amplifying character of the North Atlantic.

A review of long-term cyclic fluctuations on the century time scale is given by Stocker and Mysak (1992). Cycles of 50 years and longer are abundant in high-resolution proxy records (Fig. 25), but a clear and unequivocal time scale is missing. As an example we mention the study of Briffa *et al.* (1992) who have spectrally analyzed their 1480-year long tree ring record of Fennoscandia from which summer temperatures are reconstructed. They find significant power in the band of 30–40 years. An interesting feature is the fact that the periods are not stable: they vary by several years depending on the sub-interval considered. Such behavior is not expected if the oscillation were due to external forcing at a fixed period but rather suggests an internal mechanism.

Important insight can be gained from a synthesis of *different* paleoclimatic archives. The study of Mann *et al.* (1995) combines 35 different proxy records (tree rings, ice and coral cores, lake varves, historical records) distributed mainly in the northern hemisphere with a few "stations" in the south and covering the last 500 years. Spatial correlations and patterns of natural variability can be recognized and significant cycles in the interdecadal (15-35 years) and century (50-150 years) band are found. Interestingly, they are not stable throughout time.

The North Atlantic region appears to be a focal area of climate variability. This is also evident from recent modeling results. Decadal-to-century time scale variability does in most cases include the ocean circulation, in particular the thermohaline component. Mechanisms are connected with the wind-driven circulation as well as with the ocean/atmosphere hy-

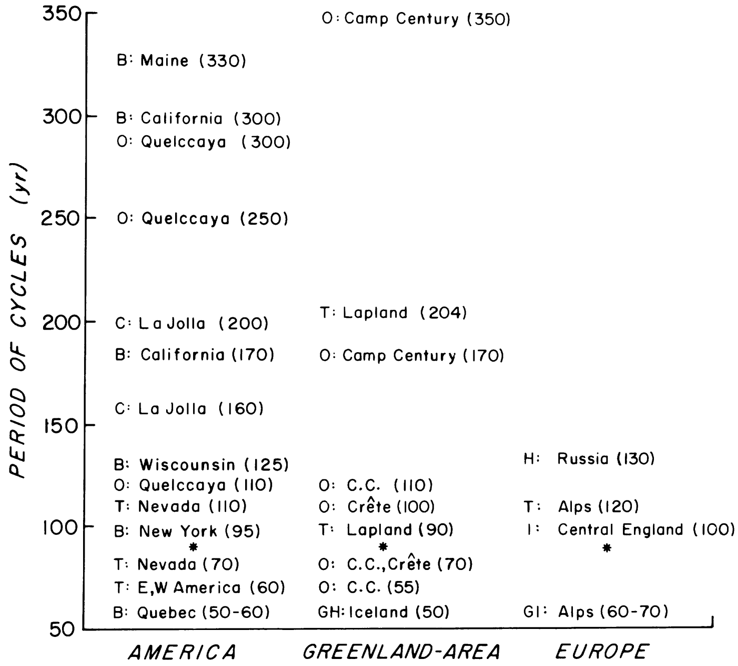

Figure 25: Summary of climatic variations observed on the century time scale. The findings are spatially and temporally ordered. The capital letters denote evidence in biological (B), radio carbon (C), glaciological (G), historical (H), instrumental (I), oxygen isotope and other ice core parameters (O) and tree ring records (T). The observed cycle period is given in brackets. C.C. denotes the Camp Century δ^{18}O record and $*$ indicates the 83-yr cycle in marine air and sea surface temperatures from Folland *et al.* (1984). [From Stocker *et al.* 1992]

drological cycle. A qualitative understanding of internal variability in the climate system is slowly emerging and centers of action have been identified.

4.3 Models and Mechanisms

The basic mechanism for oscillations due to different feedback processes of SST and SSS anomalies was summarized by Welander (1986). He showed that a circular convection loop can exhibit self-sustained oscillations when it is heated and "salted" on one side and cooled and freshened on the other. This is reminiscent of the low and high latitudes where the surface ocean is heated and evaporation causes an increase in salinity, whereas the opposite happens in the high latitudes (see Fig. 13). In 2- and 3-dimensional ocean models mechanisms generating natural variability are more difficult to understand, and the range of mechanisms and time scales is quite broad. The spectral properties of coupled atmosphere-ocean general circulation models are already exhibiting a remarkable similarity with observations (Fig. 26). However, we do not yet have a unifying theory explaining natural variability on the decadal-to-millenia time scale but are rather in the stage of collecting evidence for such fluctuations both from the observational and the modeling side. For now, a list of the type and time scales of variability found in numerical models (ocean, atmosphere, coupled) helps us in discussing physically plausible mechanisms of variability.

Table 3 on page 38 gives a summary of self-sustained oscillations found in a number of ocean,

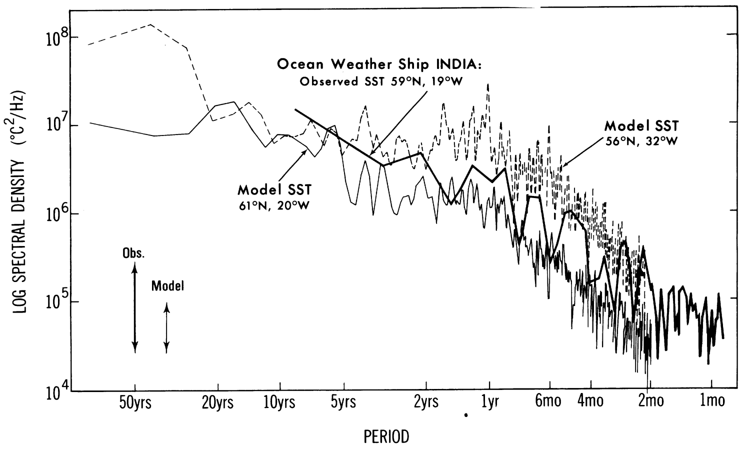

Figure 26: Comparison of the spectral properties of a coupled A-OGCM with observations. The total amount of variability in the displayed frequency band is remarkably similar to observations. [From Delworth *et al.* 1993]

atmosphere and coupled models. We focus only on the most robust cycles in these models. Mechanisms are connected mainly with the thermohaline but also with the wind-driven circulation as well as with the hydrological cycle. The table is grouped into six categories of mechanisms that will be briefly discussed below and ordered according to associated time scales. The latter is not rigorous, of course, since periods depend on model parameters. A more complete discussion is given by Stocker (1996).

a) Gyre–Thermohaline Circulation

This is a large-scale, basin-wide mechanism which is found primarily in ocean circulation models run under mixed boundary conditions (Weaver and Sarachik 1991a; Weaver *et al.* 1993; Winton and Sarachik 1993). Formed in the western boundary current, warm and saline anomalies travel eastward and are picked up by the sub-polar gyre which transports them into the region of deep water formation. There, they influence the basin-scale overturning and so feedback to the surface advection of these anomalies. While these models allow us to isolate and investigate various mechanisms of internal variability, immediate application to the real world is limited because of the simple parameterization of ocean-atmosphere interaction, simplified geometry, and their still fairly coarse resolution.

b) SST Anomalies in the Northwest Atlantic

Coupled atmosphere-ocean climate models are also beginning to exhibit natural variability. In a 600-yr run Delworth *et al.* (1993) find natural variability whose spectral properties are remarkably similar to observations (Fig. 26). Interdecadal oscillations of 40–60 yr are evident in the meridional overturning of the North Atlantic. When the thermohaline circulation is weak, decreased advection of lower-latitude warm and saline waters into the central regions of the North Atlantic generates a pool of anomalously cold and fresh water. The thermal anomaly dominates and hence generates a geostrophically controlled cyclonic circulation at the surface (baroclinic vortex). The western half of this anomalous circulation enhances

Model Type	Geometry	Perturbation	Surface Flux Parameterisation
Gyre–Thermohaline Circulation			
B&C 3D OGCM	box, flat, hemisph.	–	mixed
B&C 3D OGCM	1 sector ocean, flat, fixed ACC	var induced by mismatch of sfc heat flux and heat storage	temp. restoring time of 1-2 yr, salt flux constant
3D B&C OGCM	box, flat, hemisph.	increase of freshwater flux	freshwater flux only, no thermal forcing
B&C 3D OGCM	1 sector flat ocean, ACC fix	var induced by mismatch of sfc fluxes	mixed, constant heat or freshwater fluxes
3D OGCM	hemispheric box	–	mixed
3D OGCM	hemispheric box	–	mixed
SST Anomalies in the Northwest Atlantic			
3D A/OGCM	global	–	coupled, flux correction
3D OGCM	hemispheric box	–	constant heat flux, mixed or simple atm.
Marginal Seas			
B&C 3D OGCM	flat N Atl. and Labrador Sea	stochastic freshwater flux	mixed
3D LSG OGCM	global, incl. topography	stochastic freshwater flux	mixed
Basin-Scale Thermohaline Circulation			
2D, zonally av. OCM	1 sector ocean	stochastic freshwater flux	mixed
3D LSG OGCM	global, incl. topography	stochastic freshwater flux	mixed
The Southern Ocean-North Atlantic Connection			
3D LSG OGCM	global, topography	modified constant or stochastic freshwater flux	mixed
Other Mechanisms			
2D, zonally averaged OCM, ice	1 sector ocean	–	mixed
3D OGCM	hemispheric box	–	mixed
3D AGCM, coupled to LSG OGCM	global	–	coupled, flux correction
3D AGCM, dry	global, flat surface	–	surface energy balance

Table 3: Internal variability found in various models. [From Stocker 1996]

Period	Mechanism	Reference
Gyre–Thermohaline Circulation		
9	advection of SSS anomaly by subtrop. and subpolar gyres	(Weaver and Sarachik 1991a)
24	advection of SST anomalies by subtropical gyre, overturning influences exposure time of SST anomalies	(Cai and Godfrey 1995)
20–350	advection of SSS anomalies influencing overturning (transition to chaos)	(Huang and Chou 1994)
20–100	advection of SSS or SST anomalies	(Cai 1995)
250–500	succession of haloclines and flushes triggered by gyre salt transport	(Winton 1993)
$>$ **500**	advection of SSS anomalies by gyres and vertical diffusion	(Winton 1993)
SST Anomalies in the Northwest Atlantic		
40–60	baroclinic vortex in West Atlantic, meridional heat flux and local heat storage	(Delworth *et al.* 1993)
50–70	meridional heat transport and local heat storage	(Greatbatch and Zhang 1995)
Marginal Seas		
20	Labrador Sea, zonal and meridional overturning	(Weaver *et al.* 1994)
10–40	Labrador Sea operates as stochastic integrator sending SSS anomalies into N Atlantic	(Weisse *et al.* 1994)
Basin-Scale Thermohaline Circulation		
200–300	large-scale SSS advection	(Mysak *et al.* 1993)
320	large-scale SSS advection in the Atlantic around entire deep circulation loop	(Mikolajewicz and Maier-Reimer 1990)
The Southern Ocean-North Atlantic Connection		
320	halocline in ACC influences NADW, its outflow causes deep heating in ACC and triggers convection	(Pierce *et al.* 1995)
Other Mechanisms		
13.5	brine release–deep water formation–meridional heat flux feedback	(Yang and Neelin 1993)
17	ice cover–thermal insulation feedback	(Zhang *et al.* 1995)
10–20	advection of T anomalies in the Pacific	(Von Storch 1994)
5–40	chaotic nature, subtropical and mid-latitude atmospheric jets	(James and James 1992)

Table 3: Continuation from previous page. [From Stocker 1996]

the mean northward current of warm and saline waters located in the center of the Atlantic which is part of the large-scale conveyor belt circulation. The strengthened conveyor then carries more saline and warm low-latitude waters into this region. Again, the thermal contribution is stronger and creates an anomalous warm pool which is associated with anti-cyclonic circulation. The latter weakens the mean flow again, and the cycle begins anew. The oscillation is not stationary. It is intriguing that a similar instationarity of interdecadal cycles is clearly present in proxy data (Briffa *et al.* 1992; Mann *et al.* 1995). Similar natural variability is also present in an ocean-only model (Greatbatch and Zhang 1995) indicating some robustness of this mechanism.

c) Marginal Seas

Marginal seas (Labrador, Greenland-Iceland-Norwegian, Weddell Seas) are potentially very important pacemakers for self-sustained variability of the ocean circulation. Weaver *et al.* (1994) and Weisse *et al.* (1994) found oscillations which are generated in the Labrador Sea. The latter study also excites basin-scale cycles of the type discussed below. The two mechanisms differ distinctly from each other in that in the first study (Weaver *et al.* 1994), the Labrador Sea itself generates the variability by changing rates of local deep water formation, whereas in the other case (Weisse *et al.* 1994) the same region merely appears as a storage of perturbations which, once accumulated, act outside the basin. An increased resolution and, with it, a better representation of the water masses in the Labrador Sea will refine our understanding of its role in controlling the natural variability in the North Atlantic region.

d) Basin-Scale Thermohaline Circulation

Basin-scale variations of the Atlantic meridional overturning and hence meridional heat flux are possible mechanisms for century time scale variability (Mikolajewicz and Maier-Reimer 1990). Large fluctuations with a time scale of 320 years are found in the mass transport through Drake Passage and the meridional heat flux and overturning in the North Atlantic. The mechanism is associated with the long residence time of SSS anomalies. The random freshwater flux perturbations create local salinity anomalies that are advected northward by the near-surface circulation in the Atlantic until they reach and influence the deep water formation rate. Similar results were obtained for a wide range of parameters in a zonally averaged one-basin ocean circulation model driven by random freshwater fluxes (Mysak *et al.* 1993).

e) The Southern Ocean-North Atlantic Connection

Century time-scale variability can also be generated in the Southern Ocean (Pierce *et al.* 1995; Osborn 1995).The mechanism of variability is based on a newly found coupling between the hemispheres by the Atlantic thermohaline circulation. The model oscillates between two extreme states during one cycle: (i) strong deep water formation in the Southern Ocean with significant influx of Antarctic Bottom Water into the Atlantic where the thermohaline circulation is slightly weakened; (ii) halocline around Antarctica, no AABW in the Atlantic with slightly increased Atlantic overturning.

A cycle evolves as follows. When a strong halocline is present in the Southern Ocean, surface heat exchange is strongly reduced (due to stable stratification and ice cover). The warmer waters exiting from the Atlantic ocean manage to slowly heat up the subsurface Southern Ocean until it is destabilised. Convection then establishes fairly quickly all around Antarctica and reaches full strength within less than 100 years. During the following 200 years convection slowly decreases again due to the action of net precipitation in that area. The result is an asymmetric oscillation pattern. Pierce *et al.* (1995) show that this oscillation is only possible when a nonlinear equation of state is used.

The above mechanism is similar to the flushes found in many other models (Marotzke 1989; Wright and Stocker 1991; Weaver and Sarachik 1991b; Winton and Sarachik 1993) whose characteristic feature is a decoupling of the lower ocean from the surface. In contrast to these earlier studies where an entire basin had to be destabilized by *diffusion* and hence evolved on much longer time scales of order $10^3 - 10^4$ yrs, destabilisation here is due to *advection* of warmer NADW, i.e. an "efficient" process with a time scale of a few hundred years.

f) Other Mechanisms

Internal variability on the interdecadal time scale is found in simple ocean models when a thermodynamic sea ice component is included. Formation of a sea ice cover releases salt into the water column and induces convection (Yang and Neelin 1993; Zhang *et al.* 1995).

So far, we have discussed mainly oceanic processes localized in or related to the Atlantic. However, there are also recent model examples of interdecadal cycles in the Pacific and in the atmosphere alone (James and James 1992; Von Storch 1994).

5 Future Changes and Feedback Processes

5.1 Collapse of the Atlantic Thermohaline Circulation

Climate modelling suggests that the surface freshwater balance exerts a strong control on the THC in the North Atlantic (Manabe and Stouffer 1988; Stocker and Wright 1991a; Mikolajewicz and Maier-Reimer 1994) and that multiple equilibria can result (Fig. 14). In the glacial, ice sheets provided the perturbation mechanism: ice streams which surge into the Atlantic ocean may introduce enough freshwater to periodically disrupt the THC and trigger abrupt coolings. The last such event probably lead to the 8,200 yr BP cooling event (Barber *et al.* 1999; Alley *et al.* 1997; Leuenberger *et al.* 1999), but since the disintegration of all northern hemisphere ice sheets (except Greenland), such events have been absent.

However, this does not mean that the ocean-atmosphere system has now moved into a region of absolute stability. Warmer air temperatures, such as projected for the next century due to a continuing emission of greenhouse gases, are likely to enhance the hydrological cycle. This link between temperature and hydrological cycle is manifested by the methane changes during each D/O event: the warming is associated with a 50% increase in the CH_4 concentration whose source areas are the mid and high northern latitudes (Dällenbach *et al.* 2000). This is consistent with the notion that relatively warmer climate would cause

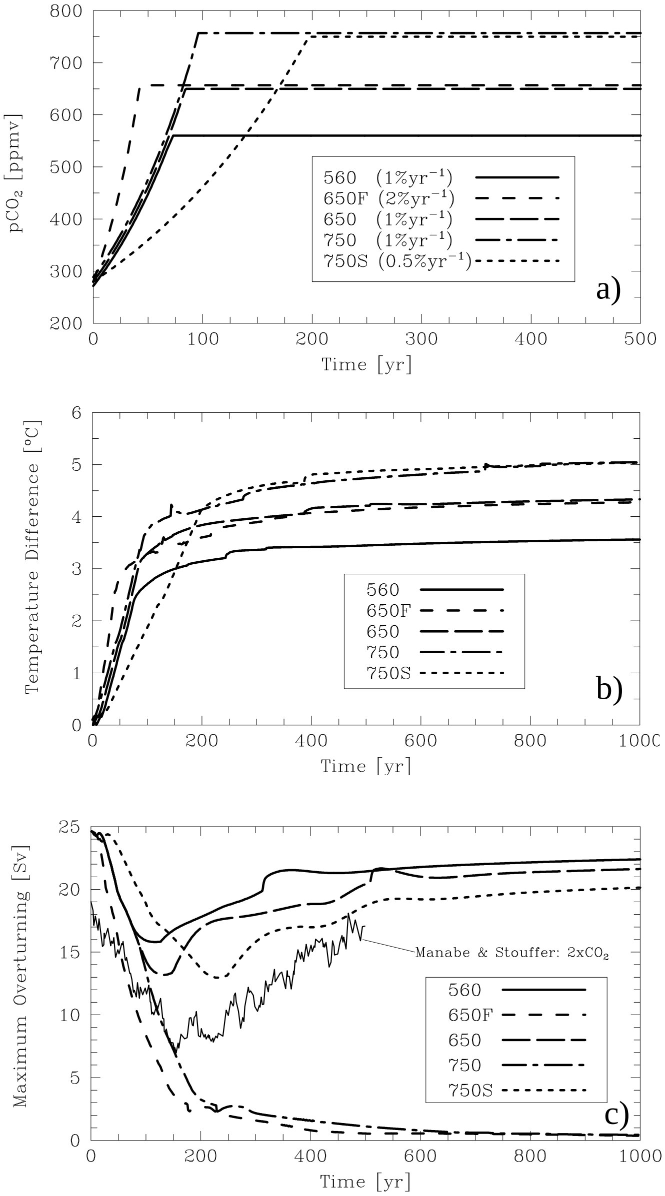

Figure 27: a: Prescribed evolution of atmospheric CO_2 for five global warming experiments. **b:** Simulated global mean surface air temperature changes. The climate sensitivity for a doubling of CO_2 was set at 3.7°C in agreement with the simulation of Manabe and Stouffer (1993). **c:** Evolution of the maximum meridional overturning of the North Atlantic in Sverdrup ($1\,\mathrm{Sv}= 10^6\mathrm{m}^3/\mathrm{s}$). Note the good agreement between the overturning simulated in the simplified model with that of the 3D AOGCM. [modified from Stocker and Schmittner 1997]

a stronger meridional moisture transport.

In summary, warming would tend to strengthen evaporation at low latitudes, increase precipitation at higher latitudes and thus accelerate the hydrological cycle. As ocean models indicate, this would lead to a reduction of deep water formation in the northern North Atlantic due to a freshening of the surface waters. A reduction of sea surface density is also caused by the increased surface air temperatures further reducing the thermohaline circulation. While the relative strength of these two mechanisms is debated (Dixon *et al.*

1999; Mikolajewicz and Voss 2000), a general reduction of the Atlantic THC in response to global warming appears to be a robust result found by the entire hierarchy of climate models (IPCC 2001).

As already Fig. 14 suggests, threshold values of key climate variables exist beyond which the THC can no longer be sustained. Among these are the level of greenhouse gases in the atmosphere (Manabe and Stouffer 1993) as well as the rate of increase of greenhouse gas concentration (Stocker and Schmittner 1997; Stouffer and Manabe 1999). This is illustrated in Fig. 27.The climate sensitivity is set at 3.7°C for a doubling of CO_2 in agreement with Manabe and Stouffer (1993). The standard rate of CO_2 increase is 1%/yr compounded; experiments with a fast rate of 2%/yr (denoted F) and a slow rate of 0.5%/yr (denoted S) are also performed. The maximum CO_2 values are 560 ppmv (exp. 560), 650 ppmv for experiments 650 and 650F, and 750 ppmv for experiments 750 and 750S. Once the maximum value is reached, CO_2 is held constant (Fig. 27a).

Simulated global mean surface air temperature changes do not depend on the emission history for a given maximum CO_2 concentration (Fig. 27b). However, there exists a bifurcation point for the maximum meridional overturning of the North Atlantic (Fig. 27c). In all cases, a reduction is obtained with an amplitude depending on the values of maximum atmospheric CO_2 and of the rate of CO_2 increase. The circulation collapses permanently for a maximum concentration of 750 ppmv with an increase at a rate of 1%/yr (exp. 750). It recovers, however, and settles to a reduced value if the increase is slower (0.5%/yr, exp. 750S) or if the final CO_2 level is reduced to 650 ppmv (exp. 650). Similarly, for a fast increase (exp. 650F) at a rate of 2%/yr the circulation collapses. All experiments have been integrated for 10,000 years and no further changes have been observed. In other words, once the THC collapses it settles to a new equilibrium and changes are hence irreversible.

The few model simulations show, that the critical level for THC collapse is somewhere between double and fourfold preindustrial CO_2 concentration, but this depends critically on various model parameterizations (Schmittner and Stocker 1999; Knutti *et al.* 2000). The threshold lies lower if the CO_2 increase is faster. If the threshold is crossed, a complete collapse of the Atlantic THC ensues which results in regional cooling and water mass reorganization very similar to the paleoclimatic experiments with the same model.

Most 3-D simulations indicate a reduction of the THC by the year 2060, but not a complete collapse (IPCC 2001). A collapse appears therefore unlikely to occur by 2100 but it can not be ruled out for later. Important in this context is to note that a reduction of the THC moves the system closer to the threshold and the likelihood of a collapse may well increase (Tziperman 2000). Concern for this potentially irreversible phenomenon may thus increase in the future.

5.2 Impact of the Projected Sea Level Rise

The Atlantic THC is an important transport mechanism from the surface to the depth. The amount of heat mixed into the interior of the ocean therefore depends also on the strength of the THC. A stronger THC would represent a more efficient downward transport of heat. More than half of the projected sea level rise is due to the thermal expansion of the water column (IPCC 1996). Because the vertical distribution of excess heat affects sea level, changes of the THC have the potential to influence the rate of sea level rise as well

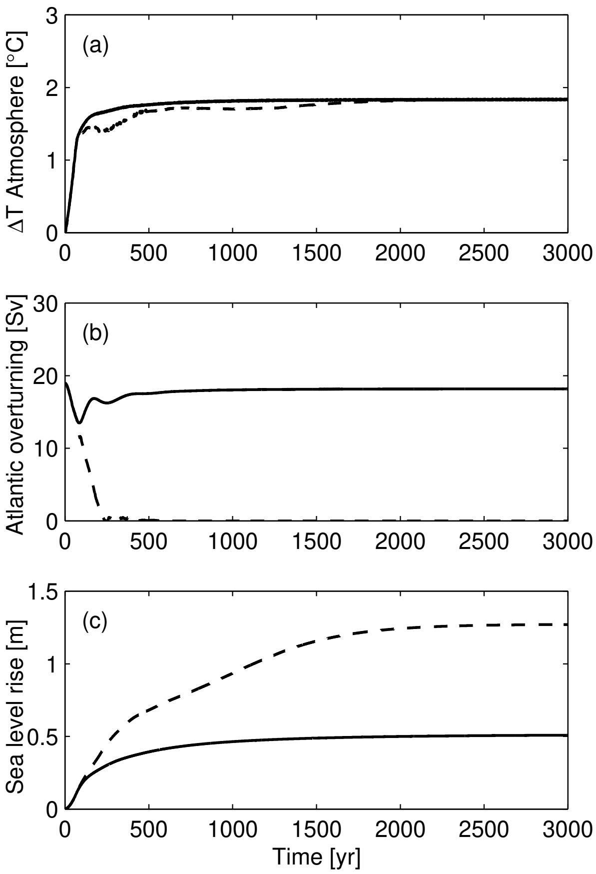

Figure 28: (a) Global mean atmospheric temperature increase, (b) Atlantic deep overturning, and (c) global mean sea level rise versus time in two almost identical global warming experiments using the model version with a Gent&McWilliams mixing scheme. If the Atlantic deep overturning collapses (dashed lines), steric sea level rise is much larger for the same atmospheric temperature increase than if the overturning recovers (solid lines). [From Knutti and Stocker 2000]

as that achieved under equilibrium.

The simplified models allow us to construct a well-defined experiment, in which the ocean model is placed at a bifurcation point. Just beyond the bifurcation point the THC collapses, otherwise it recovers. The point is that the equilibrium global warming in these two simulations is nearly identical but the internal distribution of heat may differ substantially. This is shown in Fig. 28. Global mean warming is about 1.8°C with an equilibrium sea level rise of about 0.5 m if the THC continues (solid lines, Fig. 28). However, if the circulation collapses, the equilibrium sea level rise is about 0.7 m larger. When the THC slows down, the surface waters in the North Atlantic tend to cool relative to a simulation in which the THC does not change. The increased air-sea temperature contrast therefore enhances the heat uptake during the transient phase.

5.3 A possible runaway greenhouse effect?

Given the insights about the workings of the climate system, we must pose a burning question: Do these massive ocean reorganisations have to potential to trigger a runaway

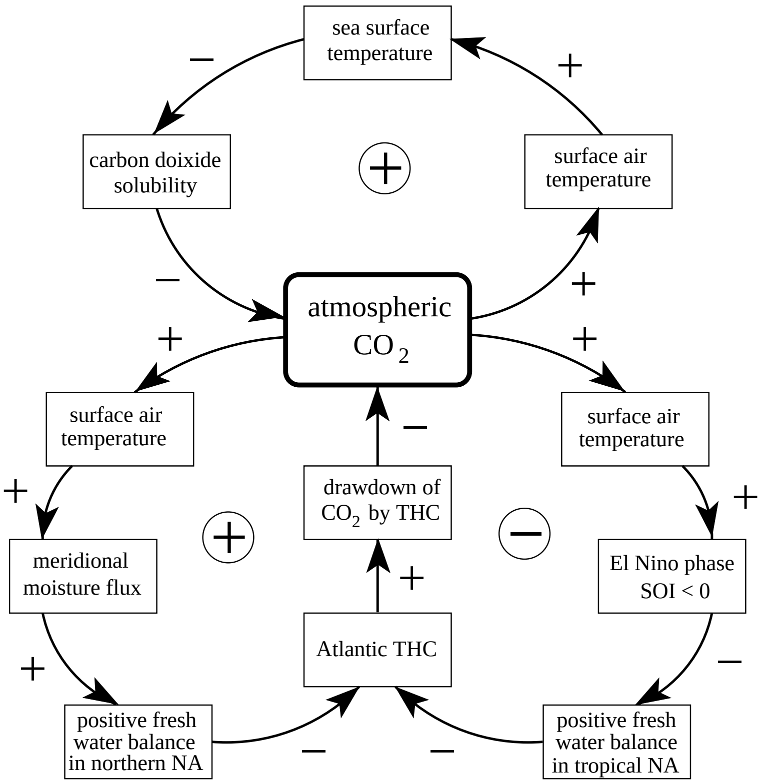

Figure 29: Possible feedback mechanisms that influence the atmospheric CO_2 concentration. In two cases, a positive feedback occurrs with the potential of reinfocing the warming. NA denotes North Atlantic, SOI is the Southern Oscillation Index.

greenhouse effect? The reasoning goes as follows (Fig. 29). A warming atmosphere clearly leads to increasing sea surface temperatures (SST) which, in turn, reduce the solubility of CO_2 in the surface waters. Warmer waters hold less dissolved carbon and warming thus causes an outgassing of this greenhouse gas. This constitutes a positive feedback loop (top in Fig. 29) enhancing the initial increase of atmospheric CO_2. A further positive feedback loop (left in Fig. 29) is associated with the effect of downward transport of carbon by the THC. If the THC collapses, much less carbon will be buried in the deep sea, again reinforcing accumulation of CO_2 in the atmosphere.

There is a third feedback loop added in Fig. 29. It is based on previous experiments which point to a stabilising effect of possible changes in ENSO as explained in section **??**. Notwithstanding, there seems enough concern to use physical-biogeochmical models to investigate quantitatively the question, how much these positive feedback mechanisms could contributed to an increase in atmospheric CO_2.

Model simulations using 3-dimensional ocean general circulation models with prescribed boundary conditions predicted a minor (Maier-Reimer *et al.* 1996) or a rather strong (Sarmiento and Le Quéré 1996) feedback between the circulation changes and the uptake of anthropogenic CO_2 under global warming scenarios. However, the complete interplay of the relevant climate system and carbon cycle components was only taken into account in the recent study by Joos *et al.* (1999). A series of CO_2 stabilization profiles were prescribed for the next 500 years along with a specific climate sensitivity, i.e. the global mean temperature increase due to a doubling of CO_2: typically 1.5–4.5°C (Fig. 30a). As expected this leads

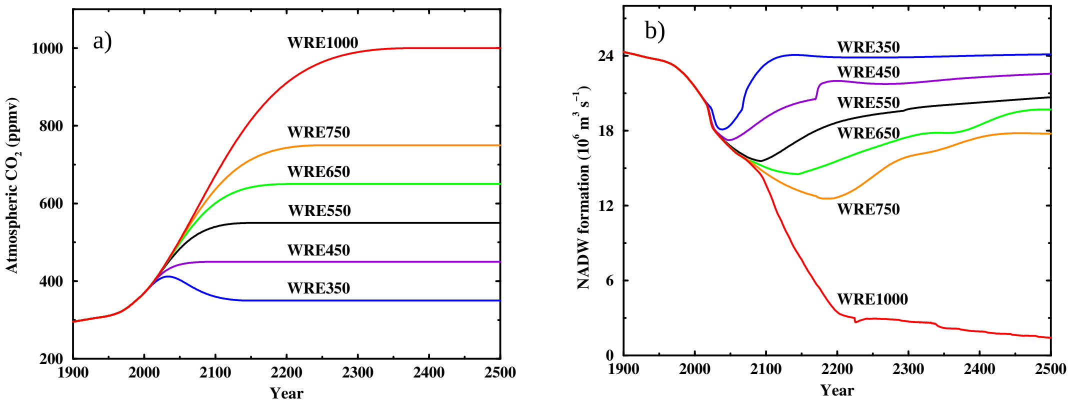

Figure 30: (a) Scenarios for the stabilization of atmospheric CO_2 concentration over the next 500 years; (b) evolution of the overturning circulation in the Atlantic in response to global warming caused by increasing concentration of CO_2. The climate sensitivity of the current experiments is 3.7°C for a doubling of CO_2 [From Joos *et al.* 1999].

to a reduction of the Atlantic THC. Again, a threshold value is between 750 and 1000 ppmv for a complete cessation of the THC (Fig. 30b).

With this model different experiments with the ocean carbon pumps operating or suppressed can be performed. Such experiments are essential for a better understanding of the various processes influencing ocean uptake of CO_2 and shown in Fig. 31. A maximum uptake of 5.5 Gt/yr is simulated if there is no change in ocean circulation nor sea surface temperature (curve A). The full simulation including all feedbacks (sea surface temperature, circulation and biota) shows a long-term reduction of almost 50% in the uptake flux provided the Atlantic THC collapses (curve B). The solubility effect is important in the first 100 years (curve C) but later, the circulation effect takes over (curve D). If the circulation does not break down as in WRE550 (Fig. 31b), circulation and biota feedback compensate each other, and the solubility effect remains the only significant feedback effect. The reduction of strength of the ocean as a major carbon sink appears a robust result, but the model also shows that dramatic feedback effects (such as a runaway greenhouse effect) are very unlikely. The maximum increase of CO_2 in the case of a collapsed Atlantic THC is estimated at about 20%. This result is entirely consistent with the evidence from the paleoclimatic records: major atmosphere-ocean reorganizations such as expected during H- or D/O-events appeared to have a relatively small influence on atmospheric CO_2 equivalent to about 30 ppm at most.

6 Conclusions

Important aspects of climate change, in particular the series of abrupt changes during the last glacial and the sequence of events that characterised the last transition from the glacial to the present warm period, are determined by chagnes in the deep circulation of the ocean. Abrupt warmings and cooling, and their counterparts in the southern hemeisphere can be explained by the operation of the Atlantic thermohaline circulation. Models suggest that

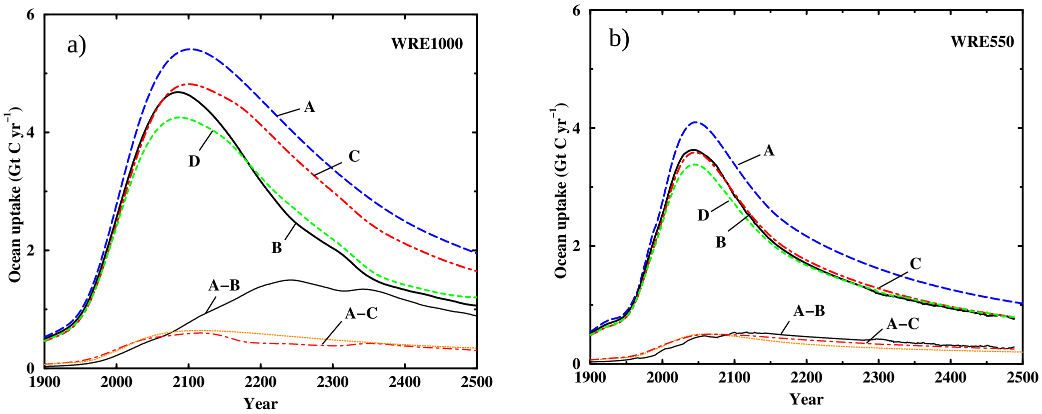

Figure 31: Evolution of the oceanic uptake of carbon dioxide for the different stabilization scenarios of Fig. 30. In WRE1000 (a), the Atlantic thermohaline circulation collapses completely by year 2500, in WRE550 (b) it remains close to the initial strength. The different simulations are labelled A–D. In A, all feedbacks are neglected (constant ocean), B is the full simulation (temperature, circulation, biota changes), C is only sea surface temperature changes (circulation held constant), D (temperature and circulation changes). Further explanations on regarding the different scenarios are in the text [From Joos *et al.* 1999].

this circulation is vulnerable to changes in the surface freshwater balance. Ice sheets have presented important sources of perturbations to the freshwater balance in the Atlantic. Frequent discharges of icebergs, which introduce massive amounts of freshwater upon melting, are recorded in marine sediments as so-called Heinrich layers. Major climatic changes are recorded in the Greenland ice cores and other high-resolution archivews around the time of these Heinrich events. Simplified models, particularly when coupled to components of biogeochemical cycles, provide a framework to study in detail the processes that are responsible for these climatic changes.

The same models also make predictions for the future. In a warmer world, the surface freshwater balance of the Atlantic will most likely be altered. Models suggest that the changes are towards more freshwater due to an enhanced meridional transport of freshwater. The thermohaline circulation reacts in the same way as it did to the iceberg perturbation: the THC reduces, in some simulations it even stops. Such changes would be massive and, although not very likely to occurr in this century, would have a profound impact on all aspects of climate, especially in the North Atlantic region. Furthermore, the same models indicate that the reduction of the THC itself moves the system closer to thresholds and instability becomes more likely.

A key task of climate research is therefore a detailed exploration of the state of the ocean-atmosphere system in order to answer the following questions:

- Is there evidence for rapid changes in warmer climates?
- What is the current state of the ocean circulation?
- Which are the thresholds and how close is the ocean-atmosphere system to them?

- How fast in in which direction is the system evolving with respect to these thresholds?

It is clear that only a very close collaboration between paleoclimatic research, observational studies in key areas and modelling using a hierarchy ranging from simplified dynamical models to 3-dimensional coupled general circulation models of the highest resolution will have the change of providing answers to these pressing questions.

Acknowledgement: I thank O. Marchal and A. Schmittner for discussions. This work was partially supported by the Swiss National Science Foundation.

References

Alley, R. B. *et al.* (1993). Abrupt increase in Greenland snow accumulation at the end of the Younger Dryas event. *Nature 362*, 527–529.

Alley, R. B., P. A. Mayewski, T. Sowers, M. Stuiver, K. C. Taylor, and P. U. Clark (1997). Holocene climatic instability: A prominent, widespread event 8200 yr ago. *Geology 25*, 483–486.

Barber, D. C., A. Dyke, C. Hillaire-Marcel, A. E. Jennings, J. T. Andrews, M. W. Kerwin, G. Bilodeau, R. McNeely, J. Southon, M. D. Morehead, and J.-M. Gagnon (1999). Forcing of the cold event of 8,200 years ago by catastrophic drainage of Laurentide lakes. *Nature 400*, 344–348.

Bard, E. *et al.* (1996). Deglacial sea-level record from Tahiti corals and the timing of global meltwater discharge. *Nature 382*, 241–244.

Baumgartner, A. and E. Reichel (1975). *The World Water Balance.* Elsevier, New York. 179 pp.

Björck, S. *et al.* (1996). Synchronised terrestrial-atmospheric deglacial records around the North Atlantic. *Science 274*, 1155–1160.

Blunier, T. *et al.* (1997). Timing of temperature variations during the last deglaciation in Antarctica and the atmospheric CO_2 increase with respect to the Younger Dryas event. *Geophys. Res. Let. 24*, 2683–2686.

Blunier, T. *et al.* (1998). Asynchrony of Antartic and Greenland climate change during the last glacial period. *Nature 394*, 739–743.

Blunier, T., J. Chappellaz, J. Schwander, B. Stauffer, and D. Raynaud (1995). Variations in the atmospheric methane concentration during the Holocene. *Nature 374*, 46–49.

Blunier, T., J. Schwander, B. Stauffer, T. Stocker, A. Dällenbach, A. Indermühle, J. Tschumi, J. Chappellaz, D. Raynaud, and J.-M. Barnola (1997). Timing of temperature variations during the last deglaciation in Antarctica and the atmospheric CO_2 increase with respect to the Younger Dryas event. *Geophys. Res. Let. 24*, 2683–2686.

Bond, G. *et al.* (1992). Evidence for massive discharges of icebergs into the North Atlantic ocean during the last glacial period. *Nature 360*, 245–249.

Bond, G. *et al.* (1993). Correlations between climate records from North Atlantic sediments and Greenland ice. *Nature 365*, 143–147.

Briffa, K. R. *et al.* (1992). Fennoscandian summers from AD 500: Temperature changes on short and long timescales. *Clim. Dyn. 7*, 111–119.

Broecker, W. S. (1991). The great ocean conveyor. *Oceanography 4*, 79–89.

Broecker, W. S. (1994). Massive iceberg discharges as triggers for global climate change. *Nature 372*, 421–424.

Broecker, W. S. (1997). Thermohaline circulation, the Achilles heel of our climate system: will man-made CO_2 upset the current balance? *Science 278*, 1582–1588.

Broecker, W. S. (1998). Paleocean circulation during the last deglaciation: a bipolar seesaw? *Paleoceanogr. 13*, 119–121.

Broecker, W. S. and G. H. Denton (1989). The role of ocean-atmosphere reorganizations in glacial cycles. *Geochim. Cosmochim. Acta 53*, 2465–2501.

Broecker, W. S., D. M. Peteet, and D. Rind (1985). Does the ocean-atmosphere system have more than one stable mode of operation? *Nature 315*, 21–25.

Bryan, F. (1986). High-latitude salinity effects and interhemispheric thermohaline circulations. *Nature 323*, 301–304.

Cai, W. (1995). Interdecadal variability driven by mismatch between surface flux forcing and oceanic freshwater/heat transport. *J. Phys. Oceanogr. 25*, 2643–2666.

Cai, W. and S. J. Godfrey (1995). Surface heat flux parameterizations and the variability of the thermohaline circulation. *J. Geophys. Res. 100*, 10679–10692.

Carissimo, B. C., A. H. Oort, and T. H. Vonder Haar (1985). Estimating the meridional energy transports in the atmosphere and oceans. *J. Phys. Oceanogr. 15*, 82–91.

Carmack, E. C. (1986). Circulation and mixing in ice-covered waters. In N. Untersteiner (Ed.), *The Geophysics of Sea Ice*, Volume B 146 of *NATO ASI*, pp. 641–712. Plenum Press.

Chamberlin, T. C. (1906). On a possible reversal of deep-sea circulation and its influence on geologic climates. *J. Geology 14*, 363–373.

Chappellaz, J., T. Blunier, D. Raynaud, J. M. Barnola, J. Schwander, and B. Stauffer (1993). Synchronous changes in atmospheric CH_4 and Greenland climate between 40 and 8 kyr BP. *Nature 366*, 443–445.

Crowley, T. J. (1992). North Atlantic deep water cools the southern hemisphere. *Paleoceanogr. 7*, 489–497.

Crowley, T. J. and K.-Y. Kim (1996). Comparison of proxy records of climate change and solar forcing. *Geophys. Res. Let. 23*, 359–362.

Dällenbach, A., T. Blunier, J. Flückiger, B. Stauffer, J. Chappellaz, and D. Raynaud (2000). Changes in the atmospheric CH_4 gradient between Greenland and Antarctica during the Last Glacial and the transition to the Holocene. *Geophys. Res. Let. 27*, 1005–1008.

Danabasoglu, G., J. C. McWilliams, and P. R. Gent (1994). The role of mesoscale tracer transports in the global ocean circulation. *Science 264*, 1123–1126.

Dansgaard, W. *et al.* (1993). Evidence for general instability of past climate from a 250-kyr ice-core record. *Nature 364*, 218–220.

Dansgaard, W., J. W. C. White, and S. J. Johnsen (1989). The abrupt termination of the Younger Dryas climate event. *Nature 339*, 532–534.

Defant, A. (1941). Quantitative Untersuchungen zur Statik und Dynamik des Atlantischen Ozeans. Die relative Topographie einzelner Druckflächen im Atlantischen Ozean. In *Wissenschaftliche Ergebnisse der Deutschen Atlantischen Expedition auf dem Forschungs- und Vermessungsschiff "Meteor" 1925–1927*, Volume 6, pp. 191–260.

Delworth, T., S. Manabe, and R. J. Stouffer (1993). Interdecadal variations of the thermohaline circulation in a coupled ocean-atmosphere model. *J. Clim. 6*, 1993–2011.

Denton, G. H. and C. H. Hendy (1994). Younger Dryas age advance of Franz Josef glacier in the southern alps of New Zealand. *Science 264*, 1434–1437.

Deser, C. and M. L. Blackmon (1993). Surface climate variations over the North Atlantic ocean during winter: 1900–1989. *J. Clim. 6*, 1743–1753.

Dickson, R. R. and J. Brown (1994). The production of North Atlantic Deep Water: Sources, rates, and pathways. *J. Geophys. Res. 99*, 12319–12341.

Dixon, K. W., T. L. Delworth, M. J. Spelman, and R. J. Stouffer (1999). The influence of transient surface fluxes on North Atlantic overturning in a coupled GCM climate change experiment. *Geophys. Res. Let. 26*, 2749–2752.

Edwards, R. L. *et al.* (1993). A large drop in atmospheric $^{14}C/^{12}C$ and reduced melting in the Younger Dryas, documented with ^{230}Th ages of corals. *Science 260*, 962–968.

Fairbanks, R. G. (1989). A 17,000 year glacio-eustatic sea-level record: Influence of glacial melting rates on the Younger Dryas event and deep ocean circulation. *Nature 342*, 637–642.

Folland, C. K., D. E. Parker, and F. E. Kates (1984). Worldwide marine temperature fluctuations 1856-1981. *Nature 310*, 670–673.

Foster, T. D. and E. C. Carmack (1976). Temperature and salinity structure in the Weddell Sea. *J. Phys. Oceanogr. 6*, 36–44.

Gent, P. R. and J. C. McWilliams (1990). Isopycnal mixing in ocean circulation models. *J. Phys. Oceanogr. 20*, 150–155.

Gent, P. R., J. Willebrand, T. J. McDougall, and J. C. McWilliams (1995). Parameterizing eddy-induced tracer transports in ocean circulation models. *J. Phys. Oceanogr. 25*, 463–474.

Gill, A. E. (1982). *Atmosphere-Ocean Dynamics*, Volume 30 of *Int. Geophys. Ser.* Academic, San Diego, Calif. 662 pp.

Gordon, A. L. (1986). Interocean exchange of thermocline water. *J. Geophys. Res. 91*, 5037–5046.

Goslar, T. *et al.* (1995). High concentration of atmospheric ^{14}C during the Younger Dryas cold episode. *Nature 377*, 414–417.

Greatbatch, R. J. and S. Zhang (1995). An interdecadal oscillation in an idealized ocean basin forced by constant heat flux. *J. Clim. 8*, 81–91.

Hammer, C. U., H. B. Clausen, and C. C. Langway (1994). Electrical conductivity method (ECM) stratigraphic dating of the Byrd Station ice core, Antarctica. *Ann. Glaciol. 20*, 115–120.

Hasselmann, K. (1976). Stochastic climate models, part I: theory. *Tellus 28*, 473–485.

Hastenrath, S. (1982). On meridional heat transports in the World Ocean. *J. Phys. Oceanogr. 12*, 922–927.

Hegerl, G. C., K. Hasselmann, U. Cubasch, J. F. B. Mitchell, E. Roeckner, R. Voss, and J. Waszkewitz (1997). Multi-fingerprint detection and attribution analysis of greenhouse gas, greenhouse gas-plus-aerosol and solar forced climate change. *Clim. Dyn. 13*, 613–634.

Huang, R. X. and R. L. Chou (1994). Parameter sensitivity study of the saline circulation. *Clim. Dyn. 9*, 391–409.

Hughen, K. A. *et al.* (1998). Deglacial changes in ocean circulation from an extended radiocarbon calibration. *Nature 391*, 65–68.

Hughes, T. M. C. and A. J. Weaver (1994). Multiple equilibria of an asymmetric two-basin ocean model. *J. Phys. Oceanogr. 24*, 619–637.

Imbrie, J., A. Berger, E. A. Boyle, S. C. Clemens, A. Duffy, W. R. Howard, G. Kukla, J. Kutzbach, D. G. Martinson, A. McIntyre, A. C. Mix, B. Molfino, J. J. Morley, L. C. Peterson, N. G. Pisias, W. L. Prell, M. E. Raymo, N. J. Shackleton, and J. R. Toggweiler (1993). On the structure and origin of major glaciation cycles, 2. the 100,000 years cycle. *Paleoceanogr. 8*, 699–735.

Imbrie, J., E. A. Boyle, S. C. Clemens, A. Duffy, W. R. Howard, G. Kukla, J. Kutzbach, D. G. Martinson, A. McIntyre, A. C. Mix, B. Molfino, J. J. Morley, L. C. Peterson, N. G. Pisias, W. L. Prell, M. E. Raymo, N. J. Shackleton, and J. R. Toggweiler (1992). On the structure and origin of major glaciation cycles, 1. linear responses to Milankovitch forcing. *Paleoceanogr. 7*, 701–738.

IPCC (1996). *Climate Change 1995, The Science of Climate Change.* Intergovernmental Panel on Climate Change, Cambridge University Press. 572 pp.

IPCC (2001). *Third Assessment Report of Climate Change*. Intergovernmental Panel on Climate Change, Cambridge University Press. in preparation.

James, I. N. and P. M. James (1992). Spatial structure of ultra-low frequency variability of the flow in a simple atmospheric circulation model. *Q. J. Roy. Met. Soc. 118*, 1211–1233.

Johnsen, S. J. *et al.* (1992). Irregular glacial interstadials recorded in a new Greenland ice core. *Nature 359*, 311–313.

Joos, F., G.-K. Plattner, T. F. Stocker, O. Marchal, and A. Schmittner (1999). Global warming and marine carbon cycle feedbacks on future atmospheric CO_2. *Science 284*, 464–467.

Kawase, M. (1987). Establishment of deep ocean circulation driven by deep water production. *J. Phys. Oceanogr. 17*, 2294–2317.

Kennet, J. P. and L. B. Ingram (1995). A 20,000-year record of ocean circulation and climate change from the Santa Barbara basin. *Nature 377*, 510–514.

Knutti, R. and T. F. Stocker (2000). Influence of the thermohaline circulation on projected sea level rise. *J. Clim. 13*, 1997–2001.

Knutti, R., T. F. Stocker, and D. G. Wright (2000). The effects of sub-grid-scale parameterizations in a zonally averaged ocean model. *J. Phys. Oceanogr. 30*, 2738–2752.

Kromer, B. and B. Becker (1993). German oak and pine ^{14}C calibration, 7200–9439 BC. *Radiocarbon 35*, 125–135.

Kushnir, J. (1994). Interdecadal variations in North Atlantic sea surface temperature and associated atmospheric conditions. *J. Clim. 7*, 141–157.

Lazier, J. R. N. (1996). The salinity decrease in the Labrador Sea over the past thirty years. In *Climate Variability on Decade-to-Century Time Scales*. National Research Council. (in press).

Lean, J. and D. Rind (1994). Solar variability: Implications for global change. *EOS, Trans. Am. Geophys. Union 75*, 1–7.

Lehman, S. J. and L. D. Keigwin (1992). Sudden changes in North Atlantic circulation during the last deglaciation. *Nature 356*, 757–762.

Leuenberger, M., C. Lang, and J. Schwander (1999). $\delta^{15}N$ measurements as a calibration tool for the paleothermometer and gas-ice age differences. A case study for the 8200 B.P. event on GRIP ice. *J. Geophys. Res. 104*, 22163–22170.

Levitus, S. (1982). Climatological atlas of the world ocean. Technical Report NOAA Prof. Pap. 13, U.S. Govt. Print. Office, Washington, D.C. 173 pp.

Levitus, S. (1989a). Interpentadal variability of salinity in the upper 150 m of the North Atlantic ocean, 1970-1974 versus 1955-1959. *J. Geophys. Res. 94*, 9679–9685.

Levitus, S. (1989b). Interpentadal variability of temperature and salinity at intermediate depths of the North Atlantic ocean, 1970-1974 versus 1955-1959. *J. Geophys. Res. 94*, 6091–6131.

Levitus, S. (1989c). Interpentadal variability of temperature and salinity in the deep North Atlantic, 1970-1974 versus 1955-1959. *J. Geophys. Res. 94*, 16125–16131.

Levitus, S. and T. P. Boyer (1994). *NOAA Atlas NESDIS 4, World Ocean Atlas 1994, Volume 4: Temperature*. NOAA, U.S. Dept. Commerce. 117 pp.

Macdonald, A. M. and C. Wunsch (1996). An estimate of global ocean circulation and heat fluxes. *Nature 382*, 436–439.

Maier-Reimer, E. and U. Mikolajewicz (1989). Experiments with an OGCM on the cause of the Younger Dryas. Technical Report 39, Max-Planck-Inst. für Meteorol., Hamburg, Germany. pp. 1–13.

Maier-Reimer, E., U. Mikolajewicz, and A. Winguth (1996). Future ocean uptake of CO_2: interaction between ocean circulation and biology. *Clim. Dyn. 12*, 711–721.

Manabe, S. and R. J. Stouffer (1988). Two stable equilibria of a coupled ocean-atmosphere model. *J. Clim. 1*, 841–866.

Manabe, S. and R. J. Stouffer (1993). Century-scale effects of increased atmospheric CO_2 on the ocean-atmosphere system. *Nature 364*, 215–218.

Mann, E., J. Park, and R. S. Bradley (1995). Global interdecadal and century-scale oscillations during the past five centuries. *Nature 378*, 266–270.

Marchal, O., T. F. Stocker, and F. Joos (1998a). Impact of oceanic reorganizations on the ocean carbon cycle and atmospheric carbon dioxide content. *Paleoceanogr. 13*, 225–244.

Marchal, O., T. F. Stocker, and F. Joos (1998b). A latitude-depth, circulation-biogeochemical ocean model for paleoclimate studies. Model development and sensitivities. *Tellus 50B*, 290–316.

Marotzke, J. (1989). Instabilities and multiple steady states of the thermohaline circulation. In D. L. T. Anderson and J. Willebrand (Eds.), *Ocean Circulation Models: Combining Data and Dynamics*, Volume C 284 of *NATO ASI*, pp. 501–511. Kluwer.

Marotzke, J. (1990). *Instabilities and Multiple Equilibria of the Thermohaline Circulation*. Ph. D. thesis, Christian-Albrechts-Universität Kiel. 126 pp.

Marotzke, J., P. Welander, and J. Willebrand (1988). Instability and multiple equilibria in a meridional-plane model of the thermohaline circulation. *Tellus 40A*, 162–172.

Marotzke, J. and J. Willebrand (1991). Multiple equilibria of the global thermohaline circulation. *J. Phys. Oceanogr. 21*, 1372–1385.

Mayewski, P. A. *et al.* (1996). Climate change during the last deglaciation in Antarctica. *Science 272*, 1636–1638.

Mikolajewicz, U. and E. Maier-Reimer (1990). Internal secular variability in an ocean general circulation model. *Clim. Dyn. 4*, 145–156.

Mikolajewicz, U. and E. Maier-Reimer (1994). Mixed boundary conditions in ocean general circulation models and their influence on the stability of the model's conveyor belt. *J. Geophys. Res. 99*, 22633–22644.

Mikolajewicz, U. and R. Voss (2000). The role of the individual air-sea flux components in CO_2-induced changes of the ocean's circulation and climate. *Clim. Dyn. 16*, 627–642.

Mitchell, J. M. (1976). An overview of climatic variability and its causal mechanisms. *Quat. Res. 6*, 481–493.

Munk, W. (1966). Abyssal recipes. *Deep Sea Res. 13*, 707–730.

Mysak, L. A., T. F. Stocker, and F. Huang (1993). Century-scale variability in a randomly forced, two-dimensional thermohaline ocean circulation model. *Clim. Dyn. 8*, 103–116.

Oceanography Course Team (1991). *I: Ocean Circulation; II: Waves, Tides and Shallow-Water Processes; III: Seawater, its composition, properties and behaviour; IV: Ocean Chemistry and Deep-Sea Sediments*. The Open University and Pergamon Press.

Oeschger, H. *et al.* (1980). ^{14}C and other parameters during the Younger Dryas cold phase. *Radiocarbon 22*, 299–310.

Oeschger, H. *et al.* (1984). Late glacial climate history from ice cores. In J. E. Hansen and T. Takahashi (Eds.), *Climate Processes and Climate Sensitivity*, Volume 29 of *Geophysical Monograph*, pp. 299–306. Am. Geophys. Union.

Osborn, T. J. (1995). *Internally-generated variability in some ocean models on decadal to millennial timescales*. Ph. D. thesis, Climatic Research Unit, School of Environmental Sciences, University of East Anglia. 404+241 pp.

Paillard, D. and L. Labeyrie (1994). Role of the thermohaline circulation in the abrupt warming after Heinrich events. *Nature 372*, 162–164.

Parilla, G., A. Lavin, H. Bryden, M. Garcia, and R. Millard (1994). Rising temperatures in the subtropical North Atlantic Ocean over the past 35 years. *Nature 369*, 48–51.

Pedlosky, J. (1987). *Geophysical Fluid Dynamics* (2 ed.). Springer. 710 pp.

Pedlosky, J. (1996). *Ocean Circulation Theory*. Springer. 453 pp.

Peixoto, J. P. and A. H. Oort (1992). *Physics of Climate.* American Institute of Physics. 500 pp.

Philander, S. G. (1990). *El Niño, La Niña, and the Southern Oscillation*, Volume 46 of *Int. Geophys. Ser.* Academic Press. 293 pp.

Pickard, G. L. and W. J. Emery (1990). *Descriptive Physical Oceanography* (5 ed.). Pergamon Press. 320 pp.

Pierce, D. W., T. P. Barnett, and U. Mikolajewicz (1995). Competing roles of heat and freshwater flux in forcing thermohaline oscillations. *J. Phys. Oceanogr. 25*, 2046–2064.

Pond, S. and G. L. Pickard (1991). *Introductory Dynamical Oceanography* (2d ed.). Pergamon Press. 329 pp.

Rahmstorf, S. (1994). Rapid climate transitions in a coupled ocean-atmosphere model. *Nature 372*, 82–85.

Rahmstorf, S. (1995). Bifurcations of the Atlantic thermohaline circulation in response to changes in the hydrological cycle. *Nature 378*, 145–149.

Redi, M. H. (1982). Oceanic isopycnal mixing by coordinate rotation. *J. Phys. Oceanogr. 12*, 1154–1158.

Reid, J. L. (1994). On the total geostrophic circulation of the North Atlantic Ocean: flow patterns, tracers, and transports. *Prog. Oceanogr. 33*, 1–92.

Roebber, P. J. (1995). Climate variability in a low-order coupled atmosphere-ocean model. *Tellus 47A*, 473–494.

Roemmich, D. and C. Wunsch (1984). Apparent changes in the climatic state of the deep North Atlantic. *Nature 307*, 447–450.

Rooth, C. (1982). Hydrology and ocean circulation. *Prog. Oceanogr. 11*, 131–149.

Ruddiman, W. F. and A. McIntyre (1981). The mode and mechanism of the last deglaciation: oceanic evidence. *Quat. Res. 16*, 125–134.

Saltzman, B. (1983). Climatic systems analysis. *Adv. Geophys. 25*, 173–233.

Sarmiento, J. L. and C. Le Quéré (1996). Oceanic carbon dioxide in a model of century-scale global warming. *Science 274*, 1346–1350.

Schlesinger, M. E. and N. Ramankutty (1994). An oscillation in the global climate system of period 65-70 years. *Nature 367*, 723–726.

Schlosser, P., G. Bönisch, M. Rhein, and R. Bayer (1991). Reduction of deepwater formation in the Greenland Sea during the 1980s: Evidence from tracer data. *Science 251*, 1054–1056.

Schmittner, A. and T. F. Stocker (1999). The stability of the thermohaline circulation in global warming experiments. *J. Clim. 12*, 1117–1133.

Schmitz, W. J. (1995). On the interbasin-scale thermohaline circulation. *Rev. Geophys. 33*, 151–173.

Stocker, T. F. (1996). An overview of century time-scale variability in the climate system: observations and models. In D. L. T. Anderson and J. Willebrand (Eds.), *Decadal Climate Variability: Dynamics and Predictability*, Volume I 44 of *NATO ASI*, pp. 379–406. Springer Verlag.

Stocker, T. F. and L. A. Mysak (1992). Climatic fluctuations on the century time scale: a review of high-resolution proxy-data. *Climate Change 20*, 227–250.

Stocker, T. F. and A. Schmittner (1997). Influence of CO_2 emission rates on the stability of the thermohaline circulation. *Nature 388*, 862–865.

Stocker, T. F. and D. G. Wright (1991a). Rapid transitions of the ocean's deep circulation induced by changes in surface water fluxes. *Nature 351*, 729–732.

Stocker, T. F. and D. G. Wright (1991b). A zonally averaged model for the thermohaline circulation. Part II: Interocean exchanges in the Pacific-Atlantic basin system. *J. Phys. Oceanogr. 21*, 1725–1739.

Stocker, T. F. and D. G. Wright (1996). Rapid changes in ocean circulation and atmospheric radiocarbon. *Paleoceanogr. 11*, 773–796.

Stocker, T. F. and D. G. Wright (1998). The effect of a succession of ocean ventilation changes on radiocarbon. *Radiocarbon 40*, 359–366.

Stocker, T. F., D. G. Wright, and L. A. Mysak (1992). A zonally averaged, coupled ocean-atmosphere model for paleoclimate studies. *J. Clim. 5*, 773–797.

Stommel, H. (1948). The westward intensification of wind-driven ocean currents. *Trans. Am. Geophys. Union 29*, 202–206.

Stommel, H. (1951). An elementary explanation of why ocean currents are strongest in the west. *Bull. Am. Met. Soc. 32*, 21–23.

Stommel, H. (1958). The abyssal circulation. *Deep Sea Res. 5*, 80–82.

Stommel, H. (1961). Thermohaline convection with two stable regimes of flow. *Tellus 13*, 224–241.

Stommel, H. (1962). On the smallness of sinking regions in the ocean. *Proc. Natl. Acad. Sci. USA 48*, 766–772.

Stommel, H. (1965). *The Gulf Stream: A Physical and Dynamical Description, 2nd edition*. Cambridge. 248 pp.

Stommel, H. and A. B. Arons (1960a). On the abyssal circulation of the world ocean - I. Stationary planetary flow patterns on a sphere. *Deep Sea Res. 6*, 140–154.

Stommel, H. and A. B. Arons (1960b). On the abyssal circulation of the world ocean - II. An idealized model of the circulation pattern and amplitude in oceanic basins. *Deep Sea Res. 6*, 217–233.

Stommel, H. and F. Schott (1977). The beta spiral and the determination of the absolute velocity field from hydrographic station data. *Deep Sea Res. 24*, 325–239.

Stouffer, R. J. and S. Manabe (1999). Response of a coupled ocean-atmosphere model to increasing atmospheric carbon dioxide: sensitivity to the rate of increase. *J. Clim. 12*, 2224–2237.

Sverdrup, H. U., M. W. Johnson, and R. H. Fleming (1942). *The Oceans: Their Physics, Chemistry, and General Biology*. Prentice-Hall. 1087 pp.

Swallow, J. C. and L. V. Worthington (1957). Measurements of deep currents in the western North Atlantic. *Nature 179*, 1183–1184.

Takahashi, T., J. Olafsson, J. G. Goddard, D. W. Chipman, and S. C. Sutherland (1993). Seasonal variation of CO_2 and nutrients in the high-latitude surface oceans: a comparative study. *Global Biogeochem. Cyc. 7*, 843–878.

Taylor, K. C. *et al.* (1993). The 'flickering switch' of late Pleistocene climate change. *Nature 361*, 432–436.

Thompson, L. G. *et al.* (1995). Late glacial stage and Holocene tropical ice core records from Huascarán, Peru. *Science 269*, 46–50.

Tziperman, E. (2000). Proximity of the present-day thermohaline circulation to an instability threshold. *J. Phys. Oceanogr. 30*, 90–104.

Veronis, G. (1981). Dynamics of large-scale ocean circulation. In B. A. Warren and C. Wunsch (Eds.), *Evolution of Physical Oceanography – Scientific Surveys in Honor of Henry Stommel*, pp. 140–183. MIT Press.

Von Storch, J. (1994). Interdecadal variability in a global coupled model. *Tellus 46A*, 419–432.

Warren, B. A. (1981). Deep circulation of the world ocean. In B. A. Warren and C. Wunsch (Eds.), *Evolution of Physical Oceanography – Scientific Surveys in Honor of Henry Stommel*, pp. 6–41. MIT Press.

Warren, B. A. and C. Wunsch (Eds.) (1981). *Evolution of Physical Oceanography – Scientific Surveys in Honor of Henry Stommel*. MIT Press. 623 pp.

Weaver, A. J., S. M. Aura, and P. G. Myers (1994). Interdecadal variability in an idealized model of the North Atlantic. *J. Geophys. Res. 99*, 12423–12441.

Weaver, A. J. and T. M. C. Hughes (1992). Stability and variability of the thermohaline circulation and its links to climate. *Trends in Phys. Oceanography 1*, 15–70.

Weaver, A. J., J. Marotzke, P. F. Cummins, and E. S. Sarachik (1993). Stability and variability of the thermohaline circulation. *J. Phys. Oceanogr. 23*, 39–60.

Weaver, A. J. and E. S. Sarachik (1991a). Evidence for decadal variability in an ocean general circulation model: an advective mechanism. *Atmosphere-Ocean 29*, 197–231.

Weaver, A. J. and E. S. Sarachik (1991b). The role of mixed boundary conditions in numerical models of the ocean's climate. *J. Phys. Oceanogr. 21*, 1470–1493.

Weisse, R., U. Mikolajewicz, and E. Maier-Reimer (1994). Decadal variability of the North Atlantic in an ocean general circulation model. *J. Geophys. Res. 99*, 12411–12422.

Welander, P. (1986). Thermohaline effects in the ocean circulation and related simple models. In J. Willebrand and D. L. T. Anderson (Eds.), *Large-Scale Transport Processes in Oceans and Atmosphere*, pp. 163–200. D. Reidel.

Winton, M. (1993). Deep decoupling oscillations of the oceanic thermohaline circulation. In W. R. Peltier (Ed.), *Ice in the Climate System*, Volume I 12 of *NATO ASI*, pp. 417–432. Springer.

Winton, M. and E. S. Sarachik (1993). Thermohaline oscillations induced by strong steady salinity forcing of ocean general circulation models. *J. Phys. Oceanogr. 23*, 1389–1410.

Wright, D. G. (1996). An equation of state for use in ocean models: Eckart's formula revisited. *J. Atm. Oceanic Technolog. 14*, 735–740.

Wright, D. G. and T. F. Stocker (1991). A zonally averaged ocean model for the thermohaline circulation, Part I: Model development and flow dynamics. *J. Phys. Oceanogr. 21*, 1713–1724.

Wright, D. G. and T. F. Stocker (1993). Younger Dryas experiments. In W. R. Peltier (Ed.), *Ice in the Climate System*, Volume I 12 of *NATO ASI*, pp. 395–416. Springer Verlag.

Wüst, G. (1935). Schichtung und Zirkulation des Atlantischen Ozeans. Die Stratosphäre. In *Wissenschaftliche Ergebnisse der Deutschen Atlantischen Expedition auf dem Forschungs- und Vermessungsschiff "Meteor" 1925–1927, 6: 1st Part, 2*, pp. 180.

Wyrtki, K. (1961). The thermohaline circulation in relation to the general circulation in the oceans. *Deep Sea Res. 8*, 39–64.

Yang, J. and J. D. Neelin (1993). Sea-ice interaction with the thermohaline circulation. *Geophys. Res. Let. 20*, 217–220.

Zbinden, H., M. Andree, H. Oeschger, B. Ammann, A. Lotter, G. Bonani, and W. Wölfli (1989). Atmospheric radiocarbon at the end of the last glacial: An estimate based on AMS radiocarbon dates on terrestrial macrofossils from lake sediments. *Radiocarbon 31*, 795–804.

Zhang, S., R. Greatbatch, and C. A. Lin (1993). A reexamination of the polar halocline catastrophe and implications for coupled ocean-atmosphere modeling. *J. Phys. Oceanogr. 23*, 287–299.

Zhang, S., C. A. Lin, and R. Greatbatch (1995). A decadal oscillation due to the coupling between an ocean circulation model and a thermodynamic sea-ice model. *J. Marine Res. 53*, 79–106.